

# Interfacial Tensions, Solubilities, and Transport Properties of the H<sub>2</sub>/H<sub>2</sub>O/NaCl System: A Molecular Simulation Study

W. A. van Rooijen,<sup>§</sup> P. Habibi,<sup>§</sup> K. Xu, P. Dey, T. J. H. Vlugt, H. Hajibeygi, and O. A. Moulton\*



Cite This: <https://doi.org/10.1021/acs.jced.2c00707>



Read Online

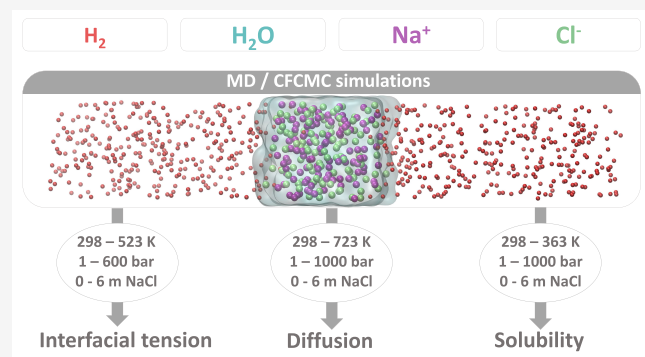
ACCESS |

Metrics & More

Article Recommendations

Supporting Information

**ABSTRACT:** Data for several key thermodynamic and transport properties needed for technologies using hydrogen (H<sub>2</sub>), such as underground H<sub>2</sub> storage and H<sub>2</sub>O electrolysis are scarce or completely missing. Force field-based Molecular Dynamics (MD) and Continuous Fractional Component Monte Carlo (CFCMC) simulations are carried out in this work to cover this gap. Extensive new data sets are provided for (a) interfacial tensions of H<sub>2</sub> gas in contact with aqueous NaCl solutions for temperatures of (298 to 523) K, pressures of (1 to 600) bar, and molalities of (0 to 6) mol NaCl/kg H<sub>2</sub>O, (b) self-diffusivities of infinitely diluted H<sub>2</sub> in aqueous NaCl solutions for temperatures of (298 to 723) K, pressures of (1 to 1000) bar, and molalities of (0 to 6) mol NaCl/kg H<sub>2</sub>O, and (c) solubilities of H<sub>2</sub> in aqueous NaCl solutions for temperatures of (298 to 363) K, pressures of (1 to 1000) bar, and molalities of (0 to 6) mol NaCl/kg H<sub>2</sub>O. The force fields used are the TIP4P/2005 for H<sub>2</sub>O, the Madrid-2019 and the Madrid-Transport for NaCl, and the Vrabec and Marx for H<sub>2</sub>. Excellent agreement between the simulation results and available experimental data is found with average deviations lower than 10%.



## 1. INTRODUCTION

Due to the vastly growing global energy demand and the resulting climate change, a transition from fossil-fuel based energy production to clean renewable energy production is crucial.<sup>1,2</sup> As a green energy carrier, hydrogen (H<sub>2</sub>) plays a crucial role in this transition because of its high gravimetric energy density and clean combustion products.<sup>3-5</sup> Important technologies in the H<sub>2</sub> value chain include underground H<sub>2</sub> storage<sup>6-9</sup> and H<sub>2</sub>O electrolysis.<sup>10,11</sup> To enable the design and optimization of these technologies, accurate knowledge of thermodynamic, interfacial, and transport properties of H<sub>2</sub> is essential.<sup>9,12-15</sup> More specifically, the diffusivities and solubilities of H<sub>2</sub> in aqueous solutions, and the interfacial tensions of H<sub>2</sub> gas in contact with aqueous electrolyte solutions are crucial properties. The interplay of these properties determines the efficiency of the technologies, and allows for accurate predictions of the processes involved, which are, e.g., required for safety. These properties depend on pressure, temperature, and salt concentration.<sup>16</sup> H<sub>2</sub> technologies cover a wide range of operational conditions. For example, in underground H<sub>2</sub> storage sites, the pressure, temperature, and salt molality can be as high as 300 bar, 333 K, and 5 mol NaCl/kg H<sub>2</sub>O, respectively.<sup>7</sup> Typically, H<sub>2</sub>O electrolyzers operate at atmospheric pressure, temperatures of ca. (348 to 372) K, and molalities of ca. (3 to 4) electrolyte/kg H<sub>2</sub>O.<sup>17,18</sup> Other types of electrolysis require much higher pressures and temperatures, i.e., up to 700 bar and 1400 K, respectively.<sup>19-21</sup> Thus, to cover the conditions for important H<sub>2</sub> applications, the

interfacial tensions, self-diffusivities, and solubilities need to be available for a very wide range of pressures, temperatures, and salt concentrations.

Traditionally, these thermophysical properties are measured experimentally.<sup>22-24</sup> Nevertheless, only a small number of experimental studies on the interfacial tension of H<sub>2</sub>/pure H<sub>2</sub>O<sup>22,25-28</sup> is available, while only two studies report measurements of interfacial tension of H<sub>2</sub>/aqueous solutions (with NaCl and NaCl+KCl).<sup>27,28</sup> These experiments are performed by using the capillary rise<sup>29</sup> and the pendant drop<sup>25,27,28,30</sup> techniques. Interfacial tensions of H<sub>2</sub>/aqueous solutions are reported for temperatures up to 423 K, pressures up to 345 bar, and molalities of up to 5 mol (NaCl + KCl)/kg H<sub>2</sub>O. As far as the solubility of H<sub>2</sub> in aqueous NaCl solutions is concerned, for an overview of the available experimental data the reader is referred to the works of Chabab et al.,<sup>31</sup> Torín-Ollarves and Trusler,<sup>32</sup> and Ansari et al.<sup>33</sup> Although a lot of experimental data are available for H<sub>2</sub> in pure H<sub>2</sub>O, solubility measurements of H<sub>2</sub> in aqueous NaCl solutions are scarce, and in many cases conflicting.<sup>23,31,34-38</sup> The two main sources of

Special Issue: In Honor of Gabriele Sadowski

Received: November 12, 2022

Accepted: December 23, 2022

experimental data of solubilities of H<sub>2</sub> in aqueous solutions at concentrations above 1 mol NaCl/kg H<sub>2</sub>O, at temperatures above 300 K, and at pressures above 10 bar by Torín-Ollarves and Trusler,<sup>32</sup> and Chabab et al.<sup>31</sup> show conflicting results as the measured solubilities differ by ca. 30%. For the self-diffusivity of H<sub>2</sub> in H<sub>2</sub>O, experimental data are available<sup>24,39–46</sup> but mostly at atmospheric pressure and for limited temperatures below 340 K. Similarly to the solubilities, the experimental measurements also differ by up to 70%. To the best of our knowledge, no experimental data are available for the self-diffusivity of H<sub>2</sub> in aqueous NaCl solutions.

Based on the available experimental data, it is evident that only a limited range of the required interfacial tensions, solubilities, and self-diffusivities of the H<sub>2</sub>/H<sub>2</sub>O/NaCl system has been measured, while in some cases, there are significant discrepancies between the data reported from different sources. The reason for the scarcity of and deviation in the data may be that experimental measurements are rather challenging and expensive to perform, especially at high pressures and temperatures. To this end, a widely used complementary approach for obtaining thermophysical data is molecular simulation, especially at conditions which are challenging for experimental measurements.

Numerous studies have used Molecular Dynamics (MD) to compute the interfacial tension of gases (e.g., CO<sub>2</sub>, CH<sub>4</sub>) and liquids (e.g., hydrocarbons) in contact with H<sub>2</sub>O (pure or saline).<sup>47–57</sup> However, no molecular simulation studies on the interfacial tension of H<sub>2</sub> and aqueous solutions are available. MD simulations have also been performed to compute self-diffusivities (i.e., self-diffusion coefficients) of H<sub>2</sub> in pure H<sub>2</sub>O.<sup>58–62</sup> Recently, Tsimpanogiannis et al.<sup>60</sup> reported such data for pressures in the range of (1 to 2000) bar and temperatures in the range of (275 to 975) K spanning vapor, liquid, and supercritical H<sub>2</sub>O. The Marx,<sup>63</sup> Vrabec,<sup>64</sup> Buch,<sup>65</sup> Hirschenfelder,<sup>66</sup> Cracknell,<sup>67</sup> and Silvera-Goldman<sup>68</sup> H<sub>2</sub> force fields were used in combination with the TIP4P/2005<sup>69</sup> H<sub>2</sub>O force field. The Buch<sup>65</sup> and Vrabec<sup>64</sup> H<sub>2</sub> force fields were shown to yield the best agreement with experimental data. In contrast, self-diffusivities of H<sub>2</sub> in aqueous NaCl solutions computed from MD simulations have not yet been reported, while there are a few studies available reporting computations of self-diffusivities of CO<sub>2</sub> in aqueous NaCl solutions.<sup>70–73</sup> Lopez-Lazaro et al.<sup>74</sup> have computed solubilities of H<sub>2</sub> in aqueous NaCl solutions using Monte Carlo (MC) simulations for molalities up to a maximum of 2 mol NaCl/kg H<sub>2</sub>O. To the best of the authors' knowledge, this was the only molecular simulation study on H<sub>2</sub> solubilities in aqueous NaCl solutions. Molecular simulations have been used for computing solubilities of other gases (e.g., CO<sub>2</sub>, CH<sub>4</sub>) in water and aqueous NaCl solutions.<sup>52,57,75–77</sup>

Despite the urgency and importance of reliable data of interfacial tension of H<sub>2</sub> in contact with aqueous NaCl solutions, self-diffusivity of H<sub>2</sub> in aqueous NaCl solutions, and solubility of H<sub>2</sub> in aqueous NaCl solutions, only very limited experimental and simulation studies are available. The objective of this work is to generate reliable data for these properties for a wide range of conditions relevant to H<sub>2</sub> technologies, such as underground H<sub>2</sub> storage and H<sub>2</sub>O electrolysis. We present new data sets of (a) interfacial tensions of H<sub>2</sub> and aqueous NaCl solutions for temperatures, pressures, and molalities of (298 to 523) K, (1 to 600) bar, and (0 to 6) mol NaCl/kg H<sub>2</sub>O, respectively, (b) self-diffusivities of H<sub>2</sub> in aqueous NaCl solutions for temperatures, pressures, and

molalities of (298 to 723) K, (1 to 1000) bar, and (0 to 6) mol NaCl/kg H<sub>2</sub>O, respectively, and (c) solubilities of H<sub>2</sub> in aqueous NaCl solutions for temperatures, pressures, and molalities of (298 to 363) K, (1 to 1000) bar and (0 to 6) mol NaCl/kg H<sub>2</sub>O, respectively. The interfacial tensions and self-diffusivities are computed using MD simulations, and the solubilities are computed using CFCMC<sup>78–80</sup> simulations. Densities and viscosities of the aqueous NaCl solutions are also computed for a wide range of conditions and are compared to available experimental data. The TIP4P/2005<sup>69</sup> force field is used for H<sub>2</sub>O, the Madrid-2019<sup>81</sup> force field for NaCl, and the Vrabec<sup>64</sup> and Marx<sup>63</sup> force fields are used for H<sub>2</sub>. A modified version of the Madrid-2019 force field by Vega and co-workers<sup>82</sup> (i.e., the Madrid-Transport<sup>77,82</sup>), optimized for viscosities of aqueous NaCl solutions for salinities up to the experimental solubility limit, is also used.

The paper is structured as follows. Details of the force fields used and the molecular simulation techniques are given in section 2. In section 3, the computed interfacial tensions, viscosities, densities, self-diffusivities, and solubilities obtained are presented and compared with experimental data when possible. Finally, concluding remarks are presented in section 4. All data computed in this study are provided in a tabulated format as Supporting Information.

## 2. METHODOLOGY

**2.1. Force Fields.** The four-site TIP4P/2005<sup>69</sup> force field is used to model H<sub>2</sub>O. Previous studies have shown that this force field can accurately capture thermodynamic, transport, and interfacial properties of pure H<sub>2</sub>O and H<sub>2</sub>O/NaCl solutions in contact with gases for a wide range of conditions.<sup>47,49,60,83–88</sup> For the Na<sup>+</sup> and Cl<sup>-</sup> ions, the Madrid-2019<sup>81</sup> force field is used, which is parametrized for the TIP4P/2005 H<sub>2</sub>O model.<sup>89</sup> A new version of the Madrid-2019 force field (i.e., Madrid-Transport force field<sup>77,82</sup>) is currently being developed by Vega and co-workers,<sup>82</sup> which performs better for transport properties, especially at high NaCl molalities. The difference of Madrid-Transport from Madrid-2019 is that ion charges are scaled by 0.75 instead of 0.85, and the Lennard-Jones (LJ) parameters are slightly altered. Interfacial tensions and self-diffusivities are computed using the single-site Vrabec<sup>64</sup> H<sub>2</sub> force field, while for the solubilities of H<sub>2</sub> in the aqueous NaCl solutions the three-site Marx<sup>63</sup> model is used. Tsimpanogiannis et al.<sup>84</sup> showed that the Vrabec<sup>64</sup> H<sub>2</sub> force field yields very accurate self-diffusivities of H<sub>2</sub> in pure TIP4P/2005 H<sub>2</sub>O. The solubilities computed using the Vrabec<sup>64</sup> force field deviate from experimental data of H<sub>2</sub> in pure water by ca. 50%. In sharp contrast, the solubilities computed using the Marx<sup>63</sup> force field show excellent agreement with experimental data. A comparison of the solubilities computed using the Marx and Vrabec force fields in pure TIP4P/2005 H<sub>2</sub>O are listed in Table S1 and shown in Figure S1 of the Supporting Information. At low temperatures, H<sub>2</sub> exhibits quantum effects which can be accounted for by using potentials such as the Feynman-Hibbs effective interaction potential.<sup>90–92</sup> At the temperatures considered in this work (i.e., 298 K and above) these quantum effects can be neglected.<sup>93</sup> All force field parameters are listed in Tables S2–S5 in the Supporting Information. A list of the chemical formulas, CAS numbers, and force fields of all species studied here is shown in Table 1.

**2.2. Molecular Simulation Details.** **2.2.1. MD Simulations.** The MD simulations are used to calculate (a) the

**Table 1.** Details of All the Species Simulated in This Work

Component	Chemical formula	CAS number	Force field
Water	H <sub>2</sub> O	7732-18-5	TIP4P/2005 <sup>69</sup>
Hydrogen	H <sub>2</sub>	133-74-0	Vrabec <sup>64</sup>
Hydrogen	H <sub>2</sub>	133-74-0	Marx <sup>63</sup>
Sodium	Na <sup>+</sup>	7440-23-5	Madrid-2019 <sup>81</sup>
Sodium	Na <sup>+</sup>	7440-23-5	Madrid-Transport <sup>77,82</sup>
Chloride	Cl <sup>-</sup>	7782-50-5	Madrid-2019 <sup>81</sup>
Chloride	Cl <sup>-</sup>	7782-50-5	Madrid-Transport <sup>77,82</sup>

interfacial tensions of H<sub>2</sub> in contact with aqueous NaCl solutions, (b) self-diffusivities of H<sub>2</sub> in aqueous NaCl solutions, (c) densities, and (d) viscosities of aqueous NaCl solutions. For all MD simulations, the Large-scale Atomic/Molecular Massively Parallel Simulator (LAMMPS)<sup>94</sup> is used (version 29 Sep 2021). For the integration of the equations of motion, the velocity-Verlet algorithm is used with a time step of 1 fs. The bond length and bending angle of H<sub>2</sub>O are fixed using the SHAKE algorithm.<sup>94,95</sup> The intermolecular interactions are described by Lennard-Jones and Coulombic interaction potentials. The Lorentz–Berthelot combining rules<sup>96</sup> are used for interactions between different types of molecules, with the exception of Na<sup>+</sup>–H<sub>2</sub>O, Na<sup>+</sup>–Cl<sup>-</sup>, and Cl<sup>-</sup>–H<sub>2</sub>O LJ interactions as specified in Table S5. Long-range electrostatic energies are computed using the particle–particle particle–mesh (PPPM) method<sup>97,98</sup> with a relative error<sup>99</sup> of 10<sup>-5</sup>. The temperature and pressure are regulated by the Nosé–Hoover thermostat and barostat.<sup>97</sup> Initial configurations are created using the PACKMOL software.<sup>100</sup> Periodic boundary conditions are imposed in all directions. All MD simulations for a specific set of conditions are repeated 5 times using different initial velocity distributions from which the average quantities are calculated. The reported uncertainties are standard deviations from the results of these 5 simulations.

**2.2.2. Computation of Interfacial Tension.** The following procedure is used for computing the interfacial tensions: An initial configuration is created by combining separately equilibrated bulk phases of aqueous sodium chloride solutions and H<sub>2</sub> gas. An equilibration run of 5 ns is carried out in the NPT ensemble using anisotropic pressure coupling, i.e., only the z-direction of the simulation box is allowed to fluctuate. The last 2 ns of the equilibration run are used to calculate the average simulation box dimensions, which are used for an equilibration run of 3 ns in the NVT ensemble. Next, production runs of 2 ns are carried out for computing the interfacial tension. In all simulations, 2088 H<sub>2</sub>O molecules are used. Depending on the pressure, the number of H<sub>2</sub> molecules varied between 64–640. 0–188 Na<sup>+</sup> and Cl<sup>-</sup> ions are used, depending on the molality. The exact numbers of species along with the simulation box sizes for all simulations are listed in Table S6 of the Supporting Information. A cutoff radius of 12 Å is used for the short-range LJ and short-range electrostatic energies. Because the system is inhomogeneous, analytic corrections were not used. Instead, long-range LJ and electrostatic interactions are computed using the Particle–Particle Particle–Mesh (PPPM) method.<sup>97,98,101</sup> For the real and reciprocal space computations for the dispersion part of the PPPM method the desired accuracies are set to 0.0001 and 0.002, respectively. A relative error of 10<sup>-5</sup> is used for the long-range electrostatic energies. The adequacy of the PPPM method for computing the LJ interactions was recently

validated by Salehi et al.<sup>102</sup> in interfacial MD simulations of deep eutectic solvents with water.

Figure 1 (top panel) shows a typical MD simulation snapshot at T = 343 K, P = 100 bar, and m = 3 mol NaCl/kg

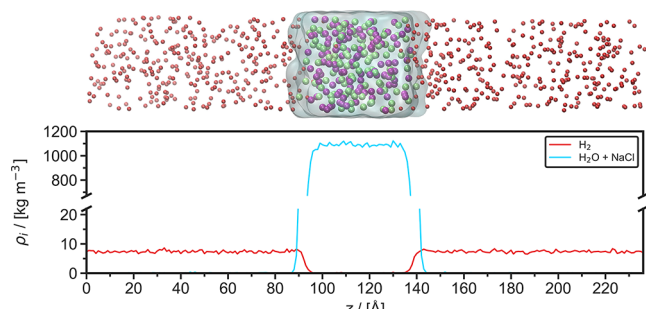


**Figure 1.** Top: Typical snapshot from a Molecular Dynamics simulation used to calculate the interfacial tension of H<sub>2</sub> and an aqueous NaCl solution (3 mol NaCl/kg H<sub>2</sub>O) at 343 K and 100 bar. H<sub>2</sub> molecules are represented by red spheres, Na<sup>+</sup> and Cl<sup>-</sup> are represented by purple and green spheres, respectively, H<sub>2</sub>O is represented by the transparent blue surface. Bottom: Density profile in the z-direction of H<sub>2</sub> and the aqueous NaCl solution of the same simulation, averaged over 1 ns. z is the direction perpendicular to the interface.

H<sub>2</sub>O. The bulk liquid H<sub>2</sub>O phase containing the Na<sup>+</sup> and Cl<sup>-</sup> ions, which is shown as the transparent blue surface, occupies a domain of ca. 40 × 40 × 40 Å<sup>3</sup> in the middle of the simulation box. H<sub>2</sub> gas is in contact with the liquid phase from both sides, in the z-direction. This creates two H<sub>2</sub>/H<sub>2</sub>O interfaces perpendicular to the z-direction. The density profile of this system, averaged over 1 ns, is shown in Figure 1 bottom panel.

The interfacial tension  $\gamma$  is calculated from the principal components of the diagonal elements of the stress tensor ( $P_{zz}$ ,  $P_{xx}$  and  $P_{yy}$ ):<sup>103</sup>

$$\gamma = \frac{1}{2} h_z \left[ P_{zz} - \frac{1}{2} (P_{xx} + P_{yy}) \right] \quad (1)$$

where  $h_z$  is the simulation cell length in the z-direction.

**2.2.3. Computation of Self-Diffusivities and Viscosities.** The scheme used for computing self-diffusivities and viscosities follows from ref 104. Initially, energy minimization of the system is performed, followed by equilibration runs in the NPT and NVT ensembles for 1–2 ns. Next, production runs in the NVT ensemble for 10 ns are carried out. The system consists of 700 H<sub>2</sub>O molecules, 2 H<sub>2</sub> molecules, and 0–76 Na<sup>+</sup> and Cl<sup>-</sup> ions, depending on the molality. The exact numbers of species used for every state point are provided in Table S7 of the Supporting Information. A cutoff radius of 10 Å is used for Lennard-Jones and electrostatic interactions. Analytic tail corrections for energies and pressures are applied.

To compute the self-diffusivities and the shear viscosities, the OCTP plugin<sup>104</sup> in LAMMPS is used. In this plugin, the Einstein relations are used in combination with the order-n algorithm<sup>97</sup> as implemented by Dubbeldam et al.<sup>105</sup> Self-diffusivity  $D_i$  of species  $i$  is computed based on the mean-squared displacements using

$$D_i = \lim_{t \rightarrow \infty} \frac{1}{6N_i t} \left\langle \sum_{j=1}^{N_i} (\mathbf{r}_{j,i}(t) - \mathbf{r}_{j,i}(0))^2 \right\rangle \quad (2)$$

where  $r_{j,i(t)}$  is the position vector of the  $j$ th molecule of species  $i$  at time  $t$  and  $N_i$  is the number of molecules of species  $i$ . All self-diffusivities in this work are corrected for finite-size effects using the Yeh-Hummer equation:<sup>106–108</sup>

$$D = D_i + \frac{k_B T \xi}{6\pi\eta L} \quad (3)$$

where  $D$  is the finite-size corrected self-diffusivity,  $T$  is the temperature in K,  $\xi$  is a dimensionless constant equal to 2.837298,  $\eta$  is the shear viscosity from eq 4, and  $L$  is the simulation box length. In this work, the finite-size correction magnitude was ca. 5–10% of the computed self-diffusivities.

Shear viscosity  $\eta$  is computed from

$$\eta = \lim_{t \rightarrow \infty} \frac{1}{10 \cdot 2t} \frac{V}{k_B T} \left\langle \sum_{\alpha\beta} \left( \int_0^t P_{\alpha\beta}^{\text{os}}(t') dt' \right)^2 \right\rangle \quad (4)$$

where

$$P_{\alpha\beta}^{\text{os}} = \frac{P_{\alpha\beta} + P_{\beta\alpha}}{2} - \delta_{\alpha\beta} \left( \frac{1}{3} \sum_k P_{kk} \right) \quad (5)$$

where  $V$  is the volume of the system,  $k_B$  is the Boltzmann constant,  $P_{\alpha\beta}^{\text{os}}$  denotes the components of the traceless pressure tensor,  $\delta_{\alpha\beta}$  is the Kronecker delta, and  $\langle \dots \rangle$  indicates an ensemble average. The computation of  $\eta$  does not depend on the size of the system.<sup>109–111</sup>

**2.2.4. Computation of Solubilities.** Continuous Fractional Component Monte Carlo<sup>78–80</sup> simulations in the isobaric–isothermal (CFCNPT) ensemble are used to compute solubilities and excess chemical potentials of H<sub>2</sub> in NaCl solutions. The open-source Brick-CFCMC software<sup>78,112,113</sup> is used for all simulations. A 10 Å cutoff radius is used for both the LJ and Coulombic interactions. The Ewald summation with a relative precision of 10<sup>-6</sup> is used for the electrostatics. Analytic tail corrections for energies and pressures are applied.<sup>97</sup> The infinite dilution excess chemical potential of H<sub>2</sub> can be computed using a single "fractional" molecule of H<sub>2</sub>. Fractional molecules have their interactions scaled with a continuous order parameter  $\lambda$ .<sup>78,93</sup> In CFCNPT simulations,  $\lambda$  ranges from 0 to 1.  $\lambda = 0$  indicates that the fractional molecule does not interact with the surrounding molecules/atoms (i.e., the fractional molecule behaves as an ideal gas molecule), and  $\lambda = 1$  corresponds to full interactions. For the specifics regarding the scaling of the interactions the reader is referred elsewhere.<sup>114–116</sup> To improve the sampling in the  $\lambda$ -space, a biasing weight function ( $W(\lambda)$ ) is created using the Wang–Landau algorithm.<sup>117,118</sup> This biasing weight function is used to ensure a flat probability distribution in the  $\lambda$ -space ( $p_{\text{obs}}(\lambda)$ ). To compute the probability of occurrence of each  $\lambda$  value, a histogram with 100 bins is used. The Boltzmann averaged probability distributions of  $\lambda$  ( $p(\lambda)$ ) can be computed using<sup>77,119</sup>

$$p(\lambda) = \frac{\langle p_{\text{obs}}(\lambda) \exp[-W(\lambda)] \rangle}{\langle \exp[-W(\lambda)] \rangle} \quad (6)$$

The Boltzmann sampled probability distribution of  $\lambda$  ( $p(\lambda)$ ) can be related to the infinite dilution chemical potential ( $\mu^{\text{ex}}$ ) using<sup>77,78,119</sup>

$$\mu^{\text{ex}} = -k_B T \ln \frac{p(\lambda = 1)}{p(\lambda = 0)} \quad (7)$$

where  $p(\lambda = 1)$  and  $p(\lambda = 0)$  are the Boltzmann averaged probability distributions of  $\lambda$  at 1 and 0, respectively.

Five  $\times 10^5$  equilibration cycles, and  $5 \times 10^5$  production cycles are performed for all simulations. A cycle contains  $N$  number of trial moves, with  $N$  being the total number of molecules, with a minimum of 20. The following probabilities are used for selecting the trial moves: 35% translations, 29% rotations, 1% volume changes, 25%  $\lambda$  changes, and 10% reinsertions of the fractional molecules at random locations inside the simulation box. The maximum displacements for molecule translations, volume changes, rotations, and  $\lambda$  changes are adjusted to obtain ca. 50% acceptance. Another method that can be used to compute  $\mu^{\text{ex}}$  is the Widom's Test Particle Insertion method (WTPI).<sup>96,97,120,121</sup> In dense fluid phases WTPI yields inaccurate results compared to the CFCMC method as successful insertion of test particles is a highly unlikely event due to the significant potential energy increase in case of overlap with other particles.<sup>78,122</sup>

The solubilities of H<sub>2</sub> in aqueous NaCl solutions are computed at temperatures in the range (298 to 363) K and at H<sub>2</sub> partial pressures of 1, 10, 100, 400, and 1000 bar. At H<sub>2</sub> partial pressures of 1 and 10 bar, the H<sub>2</sub> solubilities are computed using Henry coefficients ( $H$ ):

$$H = \lim_{f_i \rightarrow 0} \frac{f_i}{\langle \rho_{\text{H}_2,\text{L}} \rangle / \rho_0} \quad (8)$$

where  $f_i$  is the fugacity of H<sub>2</sub> in the gas phase,  $\langle \rho_{\text{H}_2,\text{L}} \rangle$  is the average number density of H<sub>2</sub> in the aqueous solution in units of 1/m<sup>3</sup>, and  $\rho_0$  is a reference number density in the same unit as  $\rho_{\text{H}_2,\text{L}}$  (set to 1 molecule per m<sup>3</sup>).<sup>119</sup> At H<sub>2</sub> partial pressures of 1 and 10 bar, the fugacity coefficient of H<sub>2</sub> is assumed to be 1 (i.e., the fugacity of H<sub>2</sub> is equal to the partial pressure of H<sub>2</sub>). The validity of eq 8 at H<sub>2</sub> partial pressures of 1–100 bar is discussed in Figure S3 of the Supporting Information. From the MC simulations,  $H$  can be computed using<sup>119</sup>

$$H = \rho_0 k_B T \exp \left[ \frac{\mu_{\text{H}_2,\text{L}}^{\text{ex}}}{k_B T} \right] \quad (9)$$

where  $\mu_{\text{H}_2,\text{L}}^{\text{ex}}$  is the infinite dilution chemical potential of H<sub>2</sub> in the aqueous solution. A single fractional molecule of H<sub>2</sub>, 300 H<sub>2</sub>O molecules, and varying number of NaCl molecules depending on the molality (ranging from 0 to 6 mol NaCl/kg H<sub>2</sub>O) are used to compute  $\mu_{\text{H}_2,\text{L}}^{\text{ex}}$ . The exact numbers of ions used for each molality are listed in Table S8 of the Supporting Information. To calculate solubilities of H<sub>2</sub> in aqueous NaCl solutions at pressures of 100, 400, and 1000 bar, the chemical potentials of H<sub>2</sub> in the liquid and in the gas phase are equated at constant pressure and temperature. The chemical potential of H<sub>2</sub> in the gas phase ( $\mu_{\text{H}_2,\text{G}}$ ) is equal to<sup>97</sup>

$$\mu_{\text{H}_2,\text{G}} = \mu_{\text{H}_2}^0 + k_B T \ln \left( \frac{\langle \rho_{\text{H}_2,\text{G}} \rangle}{\rho_0} \right) + \mu_{\text{H}_2,\text{G}}^{\text{ex}} \quad (10)$$

where  $\mu_{\text{H}_2}^0$  is the reference state of the chemical potential,  $\langle \rho_{\text{H}_2,\text{G}} \rangle$  is the average number density of H<sub>2</sub> in the gas phase in units of 1/m<sup>3</sup>, and  $\mu_{\text{H}_2,\text{G}}^{\text{ex}}$  is the excess chemical potential of H<sub>2</sub> in the gas phase. At pressures above 100 bar and at temperatures between (298 to 363) K, the gas phase contains very few H<sub>2</sub>O molecules (a H<sub>2</sub>O mole fraction below 0.01).<sup>93</sup>

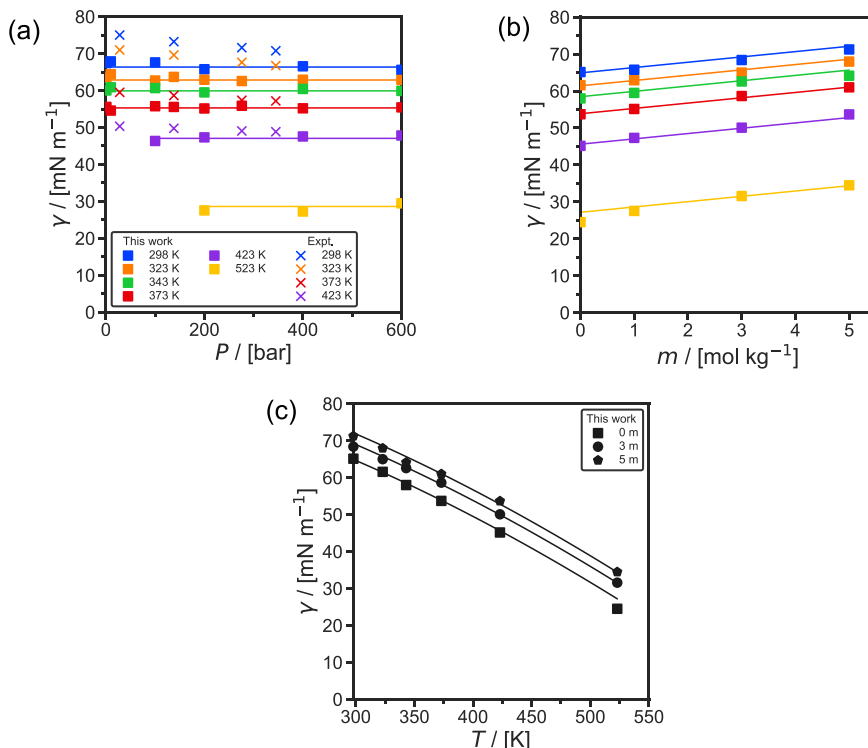


**Figure 2.** MD results of interfacial tension  $\gamma$  of  $\text{H}_2$  and aqueous  $\text{NaCl}$  solutions using the  $\text{NaCl Madrid-2019}^{81}$  force fields, the TIP4P/2005<sup>69</sup>  $\text{H}_2\text{O}$  force field, and the Vrabec<sup>64</sup>  $\text{H}_2$  force field (a) as functions of pressure  $P$  for temperatures in a range of (298 to 523) K with a molality  $m$  of 1 mol  $\text{NaCl}/\text{kg H}_2\text{O}$  in combination with the experimental results of Hosseini et al.,<sup>27</sup> (b) as functions of molality at a pressure of 200 bar of the solution for similar temperatures, and (c) as functions of temperature at a pressure of 200 bar and molalities of (0 to 6) mol  $\text{NaCl}/\text{kg H}_2\text{O}$ . The statistical uncertainties are comparable to or smaller than the symbols and can be found in Table S9 of the Supporting Information. The error bars have been omitted for clarity. The solid lines represent fits using eq 13 for temperatures in the range of (298 to 523) K.

$\mu_{\text{H}_2,\text{G}}^{\text{ex}}$  is calculated in separate CFCNPT simulations, containing a single fractional molecule of  $\text{H}_2$ , and 300  $\text{H}_2$  molecules in the gas phase. At conditions where the gas phase is nonideal and the  $\text{H}_2\text{O}$  content in the gas phase is not negligible (i.e., temperatures above 363 K and pressures above 100 bar), Gibbs ensemble simulations can be performed to simulate the gas and the liquid phase simultaneously.<sup>93</sup> These simulations are beyond the scope of this work. The chemical potential of  $\text{H}_2$  in the liquid phase ( $\mu_{\text{H}_2,\text{L}}$ ) is equal to<sup>97</sup>

$$\mu_{\text{H}_2,\text{L}} = \mu_{\text{H}_2}^0 + k_B T \ln \left( \frac{\langle \rho_{\text{H}_2,\text{L}} \rangle}{\rho_0} \right) + \mu_{\text{H}_2,\text{L}}^{\text{ex}} \quad (11)$$

$\langle \rho_{\text{H}_2,\text{L}} \rangle$  can be computed by equating eq 10 and eq 11. The mole fractions of  $\text{H}_2$  ( $x_{\text{H}_2}$ ) in aqueous  $\text{NaCl}$  solutions are computed using

$$x_{\text{H}_2} = \frac{\langle \rho_{\text{H}_2,\text{L}} \rangle \langle V \rangle}{N_{\text{H}_2\text{O}} + N_{\text{NaCl}} + \langle \rho_{\text{H}_2,\text{L}} \rangle \langle V \rangle} \quad (12)$$

where  $\langle V \rangle$  is the average volume of the simulation box, computed in the CFCNPT ensemble.  $N_{\text{H}_2\text{O}}$  and  $N_{\text{NaCl}}$  are the numbers of  $\text{H}_2\text{O}$  and  $\text{NaCl}$  molecules in the simulation box, respectively. For each condition (concentration, temperature, and pressure), 20 independent simulations are performed. These 20 simulations are divided into 5 blocks from which the Boltzmann sampled probability distributions of  $\lambda$  ( $p(\lambda)$ ) are averaged. The averaged distributions ( $p(\lambda)$ ) of all blocks are

used to compute mean values and standard deviations for the excess chemical potentials and solubilities of  $\text{H}_2$ .

### 3. RESULTS AND DISCUSSION

**3.1. Interfacial Tensions.** Figure 2 shows the computed interfacial tensions of  $\text{H}_2/\text{H}_2\text{O}/\text{NaCl}$  as a function of pressure (Figure 2a), molality (Figure 2b) at temperatures in the range of (298 to 523) K, and as a function of temperature (Figure 2c) for molalities in the range of (0 to 6) mol  $\text{NaCl}/\text{kg H}_2\text{O}$ . Tabulated raw data of the interfacial tension along with their statistical uncertainties are listed in Table S9 of the Supporting Information. Figure 2a and 2c also show the available experimental data from Hosseini et al.<sup>27</sup> For the whole range of conditions a close agreement with the experimental results is found. The MD results differ on average 6.4% from the experimental values. The simulations at 523 K cannot be directly validated due to lack of experimental data.

The interfacial tensions computed in this work are fitted to an engineering equation:

$$\gamma = c_1 + c_2 m + c_3 T^{c_4} \quad (13)$$

where  $c_1$ ,  $c_2$ ,  $c_3$ , and  $c_4$  are fitting parameters, which are listed in Table 2. Equation 13 is valid for temperatures, pressures, and molalities of (298 to 523) K, (1 to 600) bar, and (0 to 6) mol  $\text{NaCl}/\text{kg H}_2\text{O}$ , respectively. The results of this engineering equation are shown as solid lines in Figure 2. Equation 13 is a very good fit to MD results, and can be used for calculating values at a specific combination of conditions in a fast and reliable way.

**Table 2. Parameters of eq 13 for Predicting Interfacial Tension of H<sub>2</sub> in Contact with Aqueous NaCl Solutions<sup>a</sup>**

$c_1$ /[mN/m]	89.6
$c_2$ /[(mN·kg <sub>H<sub>2</sub>O</sub> )/(mol <sub>NaCl</sub> )]	1.44
$c_3$ /[mN/(m <sup>2</sup> ·K <sup>1.65</sup> )]	-2.04 × 10 <sup>-3</sup>
$c_4$ /[-]	1.65

<sup>a</sup>Values obtained using the NaCl Madrid-2019<sup>81</sup> force fields, TIP4P/2005<sup>69</sup> H<sub>2</sub>O force field, and Vrabec<sup>64</sup> H<sub>2</sub> force field. These parameters are valid for NaCl molalities of (0 to 6) mol NaCl/kg H<sub>2</sub>O, temperatures of (298 to 523) K, and pressures of (1 to 600) bar.

As shown in Figure 2a, no significant pressure dependence of interfacial tension is observed. The data of experimental studies also show no significant or small pressure dependences.<sup>22,25,27,28</sup> In particular, Higgs et al.<sup>28</sup> did not observe a significant pressure dependence for H<sub>2</sub> in contact with aqueous NaCl solutions. Other studies observed a small decrease in interfacial tension of H<sub>2</sub> and pure H<sub>2</sub>O<sup>22,25,27</sup> and H<sub>2</sub> and aqueous (NaCl+KCl) solutions.<sup>27</sup> Interestingly, the pressure dependence of H<sub>2</sub>/H<sub>2</sub>O interfacial tension is small compared to the CO<sub>2</sub>/H<sub>2</sub>O<sup>123–125</sup> and CH<sub>4</sub>/H<sub>2</sub>O<sup>51,126,127</sup> systems. This is because the interfacial tension is related to the density difference between the two phases.<sup>16</sup> The change in density difference between H<sub>2</sub> and H<sub>2</sub>O is very small at varying pressures because the density of H<sub>2</sub> is very low in comparison to H<sub>2</sub>O, and H<sub>2</sub>O is almost incompressible at these pressures.

As shown in Figure 2b, the interfacial tension increases linearly with solution molalities, in agreement with the available experimental data.<sup>27</sup> This behavior is also observed for other gases such as CO<sub>2</sub> and CH<sub>4</sub>.<sup>128–130</sup> This increase is mainly due to the increased density of saline H<sub>2</sub>O compared to pure H<sub>2</sub>O as well as the arrangement of cations and anions at the interface.<sup>129,131–135</sup> The hydrogen bond network of H<sub>2</sub>O is strengthened by cations,<sup>132–134</sup> while anions cause the opposite effect.<sup>132–134</sup> Therefore, cations are absorbed into the bulk phase while anions are depleted from the bulk phase. This phenomenon can be observed in Figure S2 of the Supporting Information, where it is shown that the number density of Cl<sup>-</sup> ions at the interface is higher than Na<sup>+</sup> ions, and Na<sup>+</sup> ions are drawn into the bulk phase. The strengthening of the hydrogen bond network of H<sub>2</sub>O leads to an increase in interfacial tension.<sup>129,131</sup>

In Figure 2c, a nonlinear decrease of interfacial tension with temperature can be observed. This is in line with the

experimental data of Chow et al.<sup>25</sup> In sharp contrast, Hosseini et al.<sup>27</sup> reported a linear decrease of interfacial tension with temperature. The fact that interfacial tension depends nonlinearly on the density difference between the two phases in contact<sup>16</sup> combined with the nonlinear effect of temperature on the density difference between H<sub>2</sub> and H<sub>2</sub>O, results in the expectation that the interfacial tension is also nonlinearly related to temperature. Therefore, the observed nonlinear relationship between interfacial tension and temperature in our results is expected.

**3.2. Viscosities and Densities.** Figure 3 shows the computed densities and viscosities of aqueous NaCl solutions as functions of NaCl molalities at 298 and 343 K. The densities are computed from the average volume calculated from the NPT ensemble. Equation 4 is used to compute the viscosities. Densities and viscosities of aqueous NaCl solutions have a weaker dependence on pressure (in the range of 0–1000 bar) compared to temperature and NaCl molalities. Figures S4 and S5 in the Supporting Information show the densities and the viscosities as functions of pressure. The results for the Madrid-2019<sup>81</sup> and the Madrid-Transport<sup>77,82</sup> NaCl force fields are shown in Figure 3. Laliberté<sup>136</sup> and Laliberté and Cooper<sup>137</sup> developed models on the basis of experimental data for viscosities and densities, respectively. These fits are shown in Figure 3. The raw data of these properties, as well as their statistical uncertainties, are listed in Table S10 of the Supporting Information. Both the Madrid-2019<sup>81</sup> and Madrid-Transport<sup>77,82</sup> capture the experimental data of density very accurately (within 1%). As shown in Figure 3a, the Madrid-Transport<sup>77,82</sup> force field yields a better agreement with the experimental data of viscosity compared to the Madrid-2019<sup>81</sup> force field. The discrepancy between the two force fields starts at molalities above 2 mol NaCl/kg H<sub>2</sub>O. The viscosities computed using the Madrid-2019 force field deviate on average ca. 20% from the experimental data, while this deviation is only ca. 3% when the Madrid-Transport force field is used. Based on the excellent performance of Madrid-Transport in reproducing experimental viscosities, which is necessary for reliable diffusivity predictions,<sup>138</sup> only this force field was used for computing the self-diffusivities of H<sub>2</sub> in NaCl solutions.

**3.3. Self-Diffusivities of H<sub>2</sub>.** Figure 4 shows the computed finite-size corrected self-diffusivities of H<sub>2</sub> in aqueous NaCl solutions as a function of (a) pressure, (b) NaCl molality, and

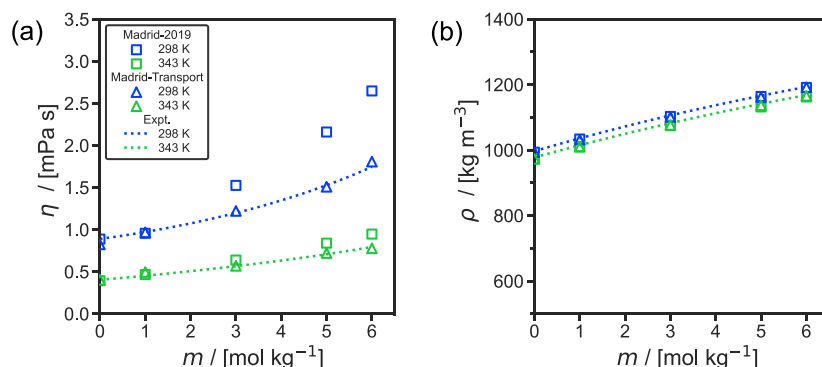


**Figure 3.** Computed (a) viscosities  $\eta$  and (b) densities  $\rho$  of aqueous NaCl solutions as a function of molality  $m$  (mol NaCl/kg H<sub>2</sub>O) at a pressure of 1 bar and temperatures of 298 and 343 K. The fit to the experimental data is created by (a) Laliberté<sup>136</sup> and (b) Laliberté and Cooper.<sup>137</sup> The statistical uncertainties can be found in Table S10 of the Supporting Information. The error bars are smaller or comparable to the symbol size and have been omitted for clarity.

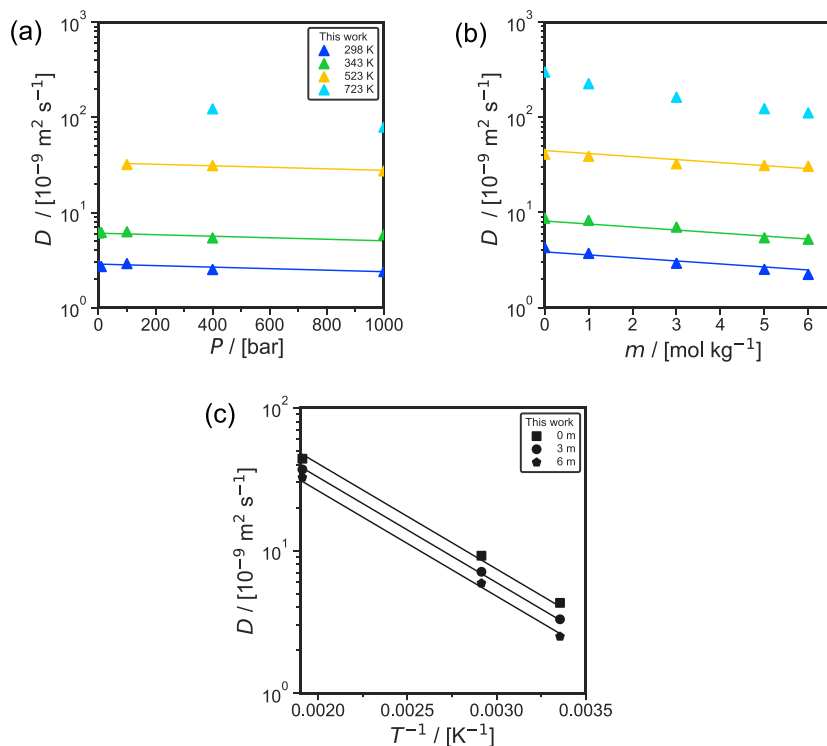


**Figure 4.** Computed finite-size corrected self-diffusivities ( $D$ ) of  $\text{H}_2$  in aqueous NaCl solutions (a) with a molality ( $m$ ) of 5 mol  $\text{NaCl}/\text{kg H}_2\text{O}$  solution as a function of pressure  $P$  for temperatures of (298 to 723) K, (b) at a pressure of 400 bar as a function of  $m$  of the solution for the similar temperatures, and (c) as a function of the reciprocal temperature at a pressure of 100 bar. The results are obtained using the NaCl Madrid-Transport<sup>77,82</sup> force fields, TIP4P/2005<sup>69</sup>  $\text{H}_2\text{O}$  force field, and Vrabec<sup>64</sup>  $\text{H}_2$  force field. The statistical uncertainties are comparable to or smaller than the symbols and can be found in Table S11 of the Supporting Information. The solid lines are fits calculated using eq 14 for temperatures of (298 to 523) K. Data points at a temperature of 723 K and a pressure of 400 bar are excluded from the fit because  $\text{H}_2\text{O}$  is supercritical at these conditions.

(c) temperature. These simulations are performed with the Madrid-Transport<sup>77,82</sup> force field for NaCl, the TIP4P/2005<sup>69</sup>  $\text{H}_2\text{O}$ , and the Vrabec<sup>64</sup> force field for  $\text{H}_2$ . All the self-diffusivities of  $\text{H}_2$  computed in this work are listed in Tables S11 and S12 of the Supporting Information. Simulations using the Madrid-2019<sup>81</sup> NaCl force field are performed for comparison. These data are shown in Table S12 of the Supporting Information.

The self-diffusivities of  $\text{H}_2$  shown in Figure 4 are fitted to an engineering correlation:

$$D = c_1 \exp \left[ c_2 m + c_3 \left( \frac{1}{T} \right) + c_4 P \right] \quad (14)$$

where  $c_1$ ,  $c_2$ ,  $c_3$ , and  $c_4$  are fitting parameters, which are listed in Table 3. As shown in Figure 4, this correlation provides an excellent fit for the MD results. Note that eq 14 is only valid for conditions at which  $\text{H}_2\text{O}$  is in the liquid phase, and therefore, data points at temperatures of 723 K or higher are excluded as the solution is in the supercritical phase. In this work, self-diffusivities for temperatures of 723 K and pressures lower than 400 bar are not calculated, because at those conditions,  $\text{H}_2\text{O}$  is in the gas phase. Equation 14 is an empirical model.

In Figure 4a a weak pressure dependence of the self-diffusivities of  $\text{H}_2$  is observed. The logarithm of the self-diffusivities decays linearly with respect to variations in pressure, similarly to what is reported by Tsimpanogiannis et al.<sup>84</sup> The pressure dependence of the self-diffusivities of  $\text{H}_2$  is more significant at 723 K (Figure 4a) as the solution is more

**Table 3. Parameters of eq 14 for Predicting the Computed Finite-Size Corrected Self-Diffusivities  $D$  of  $\text{H}_2$  in Aqueous NaCl Solutions<sup>a</sup>**

$c_1/[\text{m}^2/\text{s}]$	$1.24 \times 10^{-6}$
$c_2/[(\text{mol}_{\text{NaCl}}/\text{kg}_{\text{H}_2\text{O}})^{-1}]$	$-7.29 \times 10^{-2}$
$c_3/[\text{K}]$	$-1.70 \times 10^3$
$c_4/[\text{bar}^{-1}]$	$-1.84 \times 10^{-4}$

<sup>a</sup>Values obtained using the NaCl Madrid-Transport<sup>77,82</sup> force fields, the TIP4P/2005<sup>69</sup>  $\text{H}_2\text{O}$  force field, and the Vrabec<sup>64</sup>  $\text{H}_2$  force field. These parameters are valid for NaCl molalities of (0 to 6) mol  $\text{NaCl}/\text{kg H}_2\text{O}$ , temperatures of (298 to 523) K, and pressures of (1 to 1000) bar. Note that eq 14 should only be used at conditions in which water is in the liquid state.

compressible at these conditions. As shown in Figure 4b, the logarithm of the self-diffusivities is also found to decay linearly with respect to variation in the NaCl molalities. Laliberté<sup>136</sup> has shown that the viscosities of aqueous NaCl solutions increase exponentially with respect to NaCl molalities. As the self-diffusivities of gases dissolved in liquids are inversely proportional to the viscosities of the solution,<sup>16,138</sup> the self-diffusivities of  $\text{H}_2$  are expected to decay exponentially with respect to the NaCl molalities. The computed self-diffusivities of  $\text{H}_2$  follow an Arrhenius-type<sup>97</sup> relation with respect to variations in temperature ( $D \propto \exp \left[ \frac{c}{T} \right]$ ) as shown in Figure 4c. This behavior is also observed in literature for gases (e.g.,  $\text{O}_2$ ,  $\text{H}_2$ ) dissolved in aqueous solvents.<sup>60,86,139–141</sup>

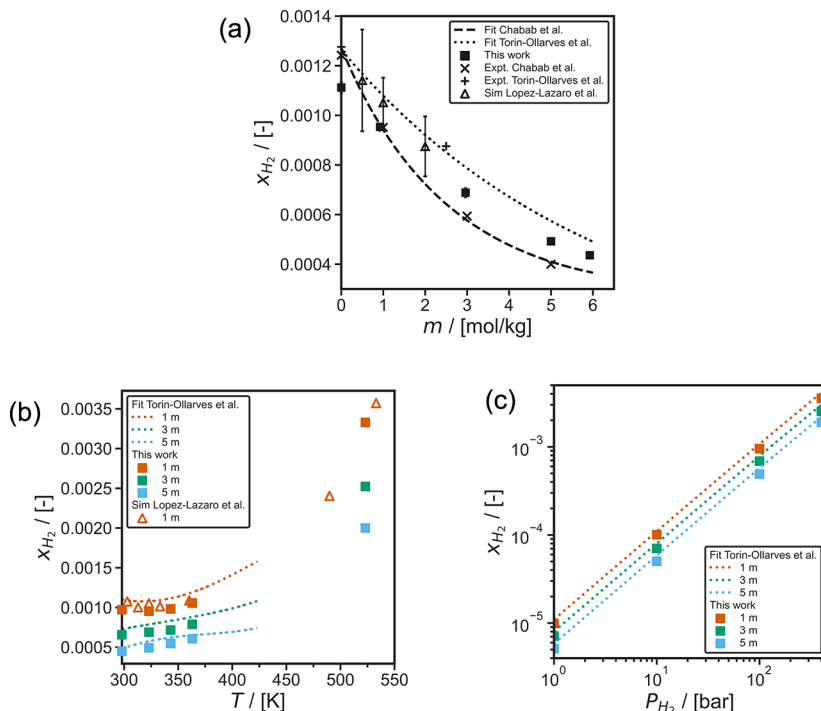


**Figure 5.** Computed solubilities of H<sub>2</sub> in aqueous NaCl solutions using the NaCl Madrid-2019 force field,<sup>81</sup> TIP4P/2005<sup>69</sup> H<sub>2</sub>O force field, and Marx<sup>63</sup> H<sub>2</sub> force field as functions of (a) NaCl molality ( $m$ ) in units of mol NaCl/kg H<sub>2</sub>O for a H<sub>2</sub> partial pressure of 100 bar, at 323 K, (b) temperature for a H<sub>2</sub> partial pressure of 100 bar, and (c) H<sub>2</sub> partial pressure at 323 K. The dashed lines represent the experimental correlation provided by Torin-Ollarves and Trusler,<sup>32</sup> and the dotted lines represent the experimental correlation results of Chabab et al.<sup>31</sup> The experimental data of Chabab et al.,<sup>31</sup> and Torin-Ollarves and Trusler,<sup>32</sup> and the simulation results of Lopez-Lazaro et al.<sup>74</sup> (converted from Henry constants) are also shown. The error bars of the simulations of this work are comparable (Figure 5a) or smaller than (Figure 5b and 5c) the symbol size.

**3.4. Solubilities.** In Figure 5, the solubilities of H<sub>2</sub> computed using CFCMC are shown as a function of (a) NaCl molality, (b) temperature, and (c) pressure. The computed solubilities are compared to the experimental measurements of Chabab et al.,<sup>31</sup> Torin-Ollarves and Trusler,<sup>32</sup> and their corresponding experimental correlations (also shown in Figure 5). The correlation of Torin-Ollarves and Trusler<sup>32</sup> is based on the experimental measurements for NaCl molalities of 0 and 2.5 mol NaCl/kg H<sub>2</sub>O, the experimental data by Wiebe and Gaddy,<sup>142</sup> Wiebe et al.,<sup>143</sup> Kling and Maurer,<sup>144</sup> and Choudhary et al.<sup>145</sup> for H<sub>2</sub> solubility in pure H<sub>2</sub>O, and the experiments by Crozier and Yamamoto<sup>37</sup> and Gordon et al.<sup>38</sup> for solubility of H<sub>2</sub> in saline solutions. Chabab et al.<sup>31</sup> provide an extensive experimental data set and a correlation for H<sub>2</sub> solubilities at temperatures of (323 to 373) K, and NaCl molalities in the range of (0 to 5) mol/kg H<sub>2</sub>O. Lopez-Lazaro et al.<sup>74</sup> obtained the Henry constants of H<sub>2</sub> in aqueous NaCl solutions for molalities up to 2 mol NaCl/kg H<sub>2</sub>O using excess chemical potentials computed using the WTPI method.<sup>96,97,120,121</sup> Using the Henry constants reported by Lopez-Lazaro et al.,<sup>74</sup> the solubilities of H<sub>2</sub> at a partial pressure of 100 bar are computed and shown in Figures 5a and 5b. The simulations of Lopez-Lazaro et al.<sup>74</sup> show large error bars (ca. 10–20%). This may be due to the use of the WTPI method,<sup>96,97,120,121</sup> which requires a large number of MC cycles to obtain low standard deviations for excess chemical potentials in the liquid phase.<sup>74,78</sup> The solubilities computed in this work using CFCMC simulations<sup>79,80,112,113</sup> have uncertainties of less than 5%.

Figure 5a shows the decrease of the solubilities of H<sub>2</sub> at increasing molalities of NaCl (i.e., salting-out effect). The

salting-out of nonpolar gases (e.g., H<sub>2</sub>, O<sub>2</sub>, and CO<sub>2</sub>) in the presence of salts such as NaCl, KCl, and KOH is a well observed phenomenon.<sup>57,77,135</sup> As shown in Figure 5a, the models by Torin-Ollarves and Trusler<sup>32</sup> and Chabab et al.<sup>31</sup> agree for H<sub>2</sub> solubilities in pure H<sub>2</sub>O and at NaCl molalities below 0.5 mol NaCl/kg H<sub>2</sub>O. For NaCl concentrations higher than 0.5 mol NaCl/kg H<sub>2</sub>O the two models predict different H<sub>2</sub> solubilities. The salting-out effect of H<sub>2</sub> observed in this work using the Madrid-2019<sup>81</sup> Na<sup>+</sup> and Cl<sup>-</sup>, TIP4P/2005<sup>69</sup> H<sub>2</sub>O, and the Marx<sup>63</sup> H<sub>2</sub> force fields shows better agreement to the salting-out effect observed by Torin-Ollarves and Trusler<sup>32</sup> as shown in Figure 5a. The correlation of Torin-Ollarves and Trusler<sup>32</sup> also shows agreement with our simulations at H<sub>2</sub> partial pressures ranging from (1 to 400) bar in the temperature range (298 to 363) K, as shown in Figures 5b and 5c. Our simulation results also agree with the MC simulations by Lopez-Lazaro et al.<sup>74</sup> both for different NaCl molalities, and for different temperatures in the range of (298 to 523) K, even though the choice of the force fields for Na<sup>+</sup>, Cl<sup>-</sup>, and H<sub>2</sub> is different. Lopez-Lazaro et al.<sup>74</sup> have used the OPLS force field<sup>146</sup> for Na<sup>+</sup>, and Cl<sup>-</sup>, combined with the model by Darkim et al.<sup>147</sup> for H<sub>2</sub>.

In Table S13 of the Supporting Information, we provide an extensive database for solubilities of H<sub>2</sub> at temperatures of (298 to 363) K, H<sub>2</sub> partial pressures of (1 to 1000) bar, and at NaCl molalities of (0 to 6) mol/kg H<sub>2</sub>O. The solubilities of H<sub>2</sub> at partial pressures up to 100 bar are computed for a wider temperature range, i.e., (298 to 523) K. These data can be further used to test and train existing machine-learning models<sup>33</sup> or equations of state<sup>148</sup> for predicting H<sub>2</sub> solubilities

in saline solutions at conditions relevant to geological H<sub>2</sub> storage.

## 4. CONCLUSIONS

Molecular simulations are used to compute (a) interfacial tensions of H<sub>2</sub> and aqueous NaCl solutions for temperatures, pressures, and molalities of (298 to 523) K, (1 to 600) bar, and (0 to 6) mol NaCl/kg H<sub>2</sub>O, respectively, (b) self-diffusivities of H<sub>2</sub> in aqueous NaCl solutions for temperatures, pressures, and molalities of (298 to 723) K, (1 to 1000) bar and (0 to 6) mol NaCl/kg H<sub>2</sub>O, respectively, and (c) solubilities of H<sub>2</sub> in aqueous NaCl solutions for temperatures, pressures, and molalities of (298 to 363) K, (1 to 1000) bar, and (0 to 6) mol NaCl/kg H<sub>2</sub>O, respectively. The simulations for computing H<sub>2</sub> self-diffusivities are also used to yield predictions for densities and viscosities of the NaCl solutions. The interfacial tensions and self-diffusivities are computed using MD simulations, and the solubilities are computed using CFCMC simulations. The H<sub>2</sub>O TIP4P/2005<sup>69</sup> force field, the NaCl Madrid-2019<sup>81</sup> force fields, and H<sub>2</sub> Vrabec<sup>64</sup> and Marx<sup>63</sup> force fields are used. In addition, a modified version of the Madrid-2019 force field (i.e., the Madrid-Transport<sup>77,82</sup> force field) is used, which is optimized for transport properties of aqueous solutions. Our results are validated against the available experimental data, models, and simulations. Excellent agreement between the results and experimental data is found with deviations smaller than 10% for the vast majority of the data points. The results of the NaCl Madrid-Transport force field were in better agreement with experimental data for transport properties, while the Madrid-2019 force field was sufficiently accurate for interfacial tensions and solubilities. The new data are used to develop engineering equations for interfacial tension and self-diffusion capturing the effect of pressure, temperature, and solution molality.

## ■ ASSOCIATED CONTENT

### § Supporting Information

The Supporting Information is available free of charge at <https://pubs.acs.org/doi/10.1021/acs.jced.2c00707>.

Solubilities of H<sub>2</sub> in pure water; force field parameters; additional info MD and CFCMC simulations; raw data MD simulations for interfacial tensions; density and viscosity data; raw data MD simulations for self-diffusivities; raw data CFCMC simulations; solubilities of H<sub>2</sub> in pure water; density profile of Na<sup>+</sup> and Cl<sup>-</sup> of a MD simulation to calculate interfacial tensions; solubilities of H<sub>2</sub> in aqueous NaCl solution at H<sub>2</sub> partial pressures of 1–100 bar; densities of NaCl solutions; viscosities of NaCl solutions ([PDF](#))

## ■ AUTHOR INFORMATION

### Corresponding Author

O. A. Moults — *Engineering Thermodynamics, Process and Energy Department, Faculty of Mechanical, Maritime and Materials Engineering, Delft University of Technology, 2628CB Delft, The Netherlands;* [orcid.org/0000-0001-7477-9684](#); Email: [o.moults@tudelft.nl](mailto:o.moults@tudelft.nl)

### Authors

W. A. van Rooijen — *Reservoir Engineering, Geoscience and Engineering Department, Faculty of Civil Engineering and*

*Geosciences, Delft University of Technology, 2628CN Delft, The Netherlands*

P. Habibi — *Engineering Thermodynamics, Process and Energy Department, Faculty of Mechanical, Maritime and Materials Engineering, Delft University of Technology, 2628CB Delft, The Netherlands; Department of Materials Science and Engineering, Faculty of Mechanical, Maritime and Materials Engineering, Delft University of Technology, 2628CD Delft, The Netherlands*

K. Xu — *Department of Materials Science and Engineering, Faculty of Mechanical, Maritime and Materials Engineering, Delft University of Technology, 2628CD Delft, The Netherlands*

P. Dey — *Department of Materials Science and Engineering, Faculty of Mechanical, Maritime and Materials Engineering, Delft University of Technology, 2628CD Delft, The Netherlands;* [orcid.org/0000-0003-4679-1752](#)

T. J. H. Vlugt — *Engineering Thermodynamics, Process and Energy Department, Faculty of Mechanical, Maritime and Materials Engineering, Delft University of Technology, 2628CB Delft, The Netherlands;* [orcid.org/0000-0003-3059-8712](#)

H. Hajibeygi — *Reservoir Engineering, Geoscience and Engineering Department, Faculty of Civil Engineering and Geosciences, Delft University of Technology, 2628CN Delft, The Netherlands*

Complete contact information is available at:  
<https://pubs.acs.org/10.1021/acs.jced.2c00707>

### Author Contributions

<sup>§</sup>W.A.v.R. and P.H. contributed equally.

### Notes

The authors declare no competing financial interest.

## ■ ACKNOWLEDGMENTS

Hadi Hajibeygi and Willemijn van Rooijen were sponsored by the Dutch National Science Foundation (NWO) Talent Programme ViDi Project “ADMIRE” (grant number 17509). This work was also sponsored by NWO Domain Science for the use of supercomputer facilities. Thijs J. H. Vlugt acknowledges NWO-CW (Chemical Sciences) for a VICI grant. O. A. Moults gratefully acknowledges the support of NVIDIA Corporation with the donation of the Titan V GPU used for this research. The authors acknowledge Carlos Vega and Samuel Blazquez for sharing the Madrid-Transport force field parameters prior to publication and for stimulating scientific discussions.

## ■ REFERENCES

- (1) World Energy Outlook 2021. 2021; [www.iea.org/weo](http://www.iea.org/weo) (accessed: 10/10/2022).
- (2) United Nations, The Paris Agreement. 2015; [https://treaties.un.org/pages/ViewDetails.aspx?src=TREATY&mtdsg\\_no=XXVII-7-d&chapter=27&clang=\\_en](https://treaties.un.org/pages/ViewDetails.aspx?src=TREATY&mtdsg_no=XXVII-7-d&chapter=27&clang=_en) (accessed: 10/10/2022).
- (3) Johnston, B.; Mayo, M. C.; Khare, A. Hydrogen: the energy source for the 21st century. *Technovation* **2005**, *25*, 569–585.
- (4) Mahlia, T.; Saktisahdan, T.; Jannifar, A.; Hasan, M.; Matseelar, H. A review of available methods and development on energy storage; technology update. *Renewable Sustainable Energy Rev.* **2014**, *33*, 532–545.
- (5) Kovač, A.; Paranos, M.; Marciuš, D. Hydrogen in energy transition: A review. *Int. J. Hydrogen Energy* **2021**, *46*, 10016–10035.

- (6) Carden, P. O.; Paterson, L. Physical, chemical and energy aspects of underground hydrogen storage. *Int. J. Hydrogen Energy* **1979**, *4*, 559–569.
- (7) Zivar, D.; Kumar, S.; Foroozesh, J. Underground hydrogen storage: A comprehensive review. *Int. J. Hydrogen Energy* **2021**, *46*, 23436–23462.
- (8) Tarkowski, R. Underground hydrogen storage: Characteristics and prospects. *Renewable Sustainable Energy Rev.* **2019**, *105*, 86–94.
- (9) Hashemi, L.; Blunt, M.; Hajibeygi, H. Pore-scale modelling and sensitivity analyses of hydrogen-brine multiphase flow in geological porous media. *Sci. Rep.* **2021**, *11*, 1–13.
- (10) Ursúa, A.; Gandia, L. M.; Sanchis, P. Hydrogen production from water electrolysis: Current status and future trends. *Proc. IEEE* **2012**, *100*, 410–426.
- (11) Grigoriev, S. A.; Fateev, V. N.; Bessarabov, D. G.; Millet, P. Current status, research trends, and challenges in water electrolysis science and technology. *Int. J. Hydrogen Energy* **2020**, *45*, 26036–26058.
- (12) Pan, B.; Yin, X.; Ju, Y.; Iglauer, S. Underground hydrogen storage: Influencing parameters and future outlook. *Adv. Colloid Interface Sci.* **2021**, *294*, 102473.
- (13) Haug, P.; Koj, M.; Turek, T. Influence of process conditions on gas purity in alkaline water electrolysis. *Int. J. Hydrogen Energy* **2017**, *42*, 9406–9418.
- (14) Haug, P.; Kreitz, B.; Koj, M.; Turek, T. Process modelling of an alkaline water electrolyzer. *Int. J. Hydrogen Energy* **2017**, *42*, 15689–15707.
- (15) Zarghami, A.; Deen, N.; Vreman, A. CFD modeling of multiphase flow in an alkaline water electrolyzer. *Chem. Eng. Sci.* **2020**, *227*, 115926.
- (16) Poling, B. E.; Prausnitz, J. M.; O'Connell, J. P. *Properties of gases and liquids*, 5th ed.; McGraw-Hill Education: New York, 2001.
- (17) Zoulias, E.; Varkarakis, E.; Lymberopoulos, N.; Christodoulou, C. N.; Karagiorgis, G. N. A review on water electrolysis. *Tcst* **2004**, *4*, 41–71.
- (18) Hnát, J.; Paidar, M.; Bouzek, K.; Iulianelli, A.; Basile, A. *Current Trends and Future Developments on (Bio-) Membranes*; Elsevier: Amsterdam, 2020.
- (19) Hauch, A.; Ebbesen, S. D.; Jensen, S. H.; Mogensen, M. Highly efficient high temperature electrolysis. *J. Mater. Chem.* **2008**, *18*, 2331–2340.
- (20) Todd, D.; Schwager, M.; Mérida, W. Thermodynamics of high-temperature, high-pressure water electrolysis. *J. Power Sources* **2014**, *269*, 424–429.
- (21) Holm, T.; Borsboom-Hanson, T.; Herrera, O. E.; Mérida, W. Hydrogen costs from water electrolysis at high temperature and pressure. *Energy Convers. Manage.* **2021**, *237*, 114106.
- (22) Slowinski, E. J.; Gates, E. E.; Waring, C. E. The effect of pressure on the surface tensions of liquids. *J. Phys. Chem.* **1957**, *61*, 808–810.
- (23) Braun, L. Über die Absorption von Stickstoff und von Wasserstoff in wässerigen Lösungen verschieden dissociierter Stoffe. *Z. Phys. Chem.* **1900**, *33U*, 721–739.
- (24) Gertz, K.; Loeschke, H. Bestimmung der Diffusions-Koeffizienten von  $H_2$ ,  $O_2$ ,  $N_2$ , und  $He$  in Wasser und Blutserum bei konstant gehaltener Konvektion. *Z. Naturforsch. B* **1954**, *9*, 1–9.
- (25) Chow, Y. T.; Maitland, G. C.; Trusler, J. P. Interfacial tensions of  $(H_2O + H_2)$  and  $(H_2O + CO_2 + H_2)$  systems at temperatures of (298–448) K and pressures up to 45 MPa. *Fluid Phase Equilib.* **2018**, *475*, 37–44.
- (26) Massoudi, R.; King, A. D., Jr Effect of pressure on the surface tension of water. Adsorption of low molecular weight gases on water at 25 °C. *J. Phys. Chem.* **1974**, *78*, 2262–2266.
- (27) Hosseini, M.; Fahimipour, J.; Ali, M.; Keshavarz, A.; Iglauer, S.  $H_2$ -brine interfacial tension as a function of salinity, temperature, and pressure; implications for hydrogen geo-storage. *J. Pet. Sci. Eng.* **2022**, *213*, 110441.
- (28) Higgs, S.; Da Wang, Y.; Sun, C.; Ennis-King, J.; Jackson, S. J.; Armstrong, R. T.; Mostaghimi, P. In-situ hydrogen wettability characterisation for underground hydrogen storage. *Int. J. Hydrogen Energy* **2022**, *47*, 13062–13075.
- (29) Richards, T. W.; Carver, E. K. A critical study of the capillary rise method of determining surface tension, with data for water, benzene, toluene, chloroform, carbon tetrachloride, ether and dimethyl aniline.[second paper.]. *J. Am. Chem. Soc.* **1921**, *43*, 827–847.
- (30) Drelich, J.; Fang, C.; White, C. Measurement of interfacial tension in fluid-fluid systems. *Encycl. Surf. Colloid Sci.* **2002**, *3*, 3158–3163.
- (31) Chabab, S.; Théveneau, P.; Coquelet, C.; Corvisier, J.; Paricaud, P. Measurements and predictive models of high-pressure  $H_2$  solubility in brine ( $H_2O + NaCl$ ) for underground hydrogen storage application. *Int. J. Hydrogen Energy* **2020**, *45*, 32206–32220.
- (32) Torín-Ollarves, G. A.; Trusler, J. M. Solubility of hydrogen in sodium chloride brine at high pressures. *Fluid Phase Equilib.* **2021**, *539*, 113025.
- (33) Ansari, S.; Safaei-Farouji, M.; Atashrouz, S.; Abedi, A.; Hemmati-Sarapardeh, A.; Mohaddespour, A. Prediction of hydrogen solubility in aqueous solutions: Comparison of equations of state and advanced machine learning-metaheuristic approaches. *Int. J. Hydrogen Energy* **2022**, *47*, 37724.
- (34) Steiner, P. Ueber die Absorption des Wasserstoffs im Wasser und in wässerigen Lösungen. *Ann. Phys.* **1894**, *288*, 275–299.
- (35) Knopp, W. Über die Löslichkeitsbeeinflussung von Wasserstoff und Stickoxydul in wässerigen Lösungen verschieden dissoziierter Stoffe. *Z. Phys. Chem.* **1904**, *48U*, 97–108.
- (36) Gerecke, J.; Bittrich, H. The solubility of  $H_2$ ,  $CO_2$  and  $NH_3$  in an aqueous electrolyte solution. *Wiss. Z. Tech. Hochsch. Chem. Carl Schorlemmer Leuna Merseburg* **1971**, *13*, 115–122.
- (37) Crozier, T. E.; Yamamoto, S. Solubility of Hydrogen in Water, Seawater, and  $NaCl$  Solutions. *J. Chem. Eng. Data* **1974**, *19*, 242–244.
- (38) Gordon, L. I.; Cohen, Y.; Standley, D. R. The solubility of molecular hydrogen in seawater. *Deep-Sea Res.* **1977**, *24*, 937–941.
- (39) Winkelmann, J. *Landolt-Bornstein: Numerical Data and Functional Relationships in Science and Technology, Group IV*, 1st ed.; Springer-Verlag: New York, 2007; Vol. 15A.
- (40) Baird, M. H. I.; Davidson, J. F. Annular jets-II: Gas absorption. *Chem. Eng. Sci.* **1962**, *17*, 473–480.
- (41) Houghton, G.; Wise, D. L. The diffusion coefficients of ten slightly soluble gases in water at 10–60 °C. *Chem. Eng. Sci.* **1966**, *21*, 999–1010.
- (42) Akgerman, A.; Gainer, J. L. Predicting gas-liquid diffusivities. *J. Chem. Eng. Data* **1972**, *17*, 372–377.
- (43) Himmelblau, D. M. Diffusion of dissolved gases in liquids. *Chem. Rev.* **1964**, *64*, 527–550.
- (44) Verhallen, P. T. H. M.; Oomen, L. J. P.; Elsen, A. J. J. M.; Kruger, J.; Fortuin, J. M. H. The diffusion coefficients of helium, hydrogen, oxygen and nitrogen in water determined from the permeability of a stagnant liquid layer in the quasi-s. *Chem. Eng. Sci.* **1984**, *39*, 1535–1541.
- (45) Jähne, B.; Heinz, G.; Dietrich, W. Measurement of the diffusion coefficients of sparingly soluble gases in water. *J. Geophys. Res.: Oceans* **1987**, *92*, 10767–10776.
- (46) De Blok, W. J.; Fortuin, J. M. H. Method for determining diffusion coefficients of slightly soluble gases in liquids. *Chem. Eng. Sci.* **1981**, *36*, 1687–1694.
- (47) Nielsen, L. C.; Bourg, I. C.; Sposito, G. Predicting  $CO_2$ -water interfacial tension under pressure and temperature conditions of geologic  $CO_2$  storage. *Geochim. Cosmochim. Acta* **2012**, *81*, 28–38.
- (48) Li, X.; Ross, D. A.; Trusler, J. P. M.; Maitland, G. C.; Boek, E. S. Molecular dynamics simulations of  $CO_2$  and brine interfacial tension at high temperatures and pressures. *J. Phys. Chem. B* **2013**, *117*, 5647–5652.
- (49) Liu, Y.; Lafitte, T.; Panagiotopoulos, A. Z.; Debenedetti, P. G. Simulations of vapor-liquid phase equilibrium and interfacial tension in the  $CO_2$ - $H_2O$ - $NaCl$  system. *AIChE J.* **2013**, *59*, 3514–3522.

- (50) Tsuji, S.; Liang, Y.; Kunieda, M.; Takahashi, S.; Matsuoka, T. Molecular Dynamics Simulations of the CO<sub>2</sub>-Water-silica Interfacial Systems. *Energy Procedia* **2013**, *37*, 5435–5442.
- (51) Knauer, S.; Schenk, M. R.; Koddermann, T.; Reith, D.; Jaeger, P. Interfacial tension and related properties of ionic liquids in CH<sub>4</sub> and CO<sub>2</sub> at elevated pressures: experimental data and molecular dynamics simulation. *J. Chem. Eng. Data* **2017**, *62*, 2234–2243.
- (52) Hosseinzadeh Dehaghani, Y.; Assareh, M.; Feyzi, F. Simultaneous Prediction of Equilibrium, Interfacial, and Transport Properties of CO<sub>2</sub>-Brine Systems Using Molecular Dynamics Simulation: Applications to CO<sub>2</sub> Storage. *Ind. Eng. Chem. Res.* **2022**, *61*, 15390–15406.
- (53) Zhao, L.; Ji, J.; Tao, L.; Lin, S. Ionic effects on supercritical CO<sub>2</sub>-brine interfacial tensions: Molecular dynamics simulations and a universal correlation with ionic strength, temperature, and pressure. *Langmuir* **2016**, *32*, 9188–9196.
- (54) Yang, Y.; Narayanan Nair, A. K.; Sun, S. Molecular dynamics simulation study of carbon dioxide, methane, and their mixture in the presence of brine. *J. Phys. Chem. B* **2017**, *121*, 9688–9698.
- (55) Papavasileiou, K. D.; Moultsos, O. A.; Economou, I. G. Predictions of water/oil interfacial tension at elevated temperatures and pressures: A molecular dynamics simulation study with biomolecular force fields. *Fluid Phase Equilib.* **2018**, *476*, 30–38.
- (56) Aminian, A.; ZareNezhad, B. Molecular dynamics simulations study on the shear viscosity, density, and equilibrium interfacial tensions of CO<sub>2</sub> + brines and brines + CO<sub>2</sub> + n-decane systems. *J. Phys. Chem. B* **2021**, *125*, 2707–2718.
- (57) Blazquez, S.; Zeron, I.; Conde, M.; Abascal, J.; Vega, C. Scaled charges at work: Salting out and interfacial tension of methane with electrolyte solutions from computer simulations. *Fluid Phase Equilib.* **2020**, *513*, 112548.
- (58) Kallikragas, D. T.; Plugatyr, A. Y.; Svishchev, I. M. High temperature diffusion coefficients for O<sub>2</sub>, H<sub>2</sub>, and OH in water, and for pure water. *J. Chem. Eng. Data* **2014**, *59*, 1964–1969.
- (59) Zhao, X.; Jin, H. Investigation of hydrogen diffusion in supercritical water: A molecular dynamics simulation study. *Int. J. Heat Mass Transfer* **2019**, *133*, 718–728.
- (60) Tsimpanogiannis, I. N.; Maity, S.; Celebi, A. T.; Moultsos, O. A. Engineering Model for Predicting the Intradiffusion Coefficients of Hydrogen and Oxygen in Vapor, Liquid, and Supercritical Water based on Molecular Dynamics Simulations. *J. Chem. Eng. Data* **2021**, *66*, 3244.
- (61) Zhao, X.; Jin, H. Correlation for self-diffusion coefficients of H<sub>2</sub>, CH<sub>4</sub>, CO, O<sub>2</sub> and CO<sub>2</sub> in supercritical water from molecular dynamics simulation. *Appl. Therm. Eng.* **2020**, *171*, 114941.
- (62) Zhao, X.; Jin, H.; Chen, Y.; Ge, Z. Numerical study of H<sub>2</sub>, CH<sub>4</sub>, CO, O<sub>2</sub> and CO<sub>2</sub> diffusion in water near the critical point with molecular dynamics simulation. *Comput. Math. with Appl.* **2021**, *81*, 759–771.
- (63) Marx, D.; Nielaba, P. Path-integral Monte Carlo techniques for rotational motion in two dimensions: Quenched, annealed, and no-spin quantum-statistical averages. *Phys. Rev. A* **1992**, *45*, 8968.
- (64) Köster, A.; Thol, M.; Vrabec, J. Molecular Models for the Hydrogen Age: Hydrogen, Nitrogen, Oxygen, Argon, and Water. *J. Chem. Eng. Data* **2018**, *63*, 305–320.
- (65) Buch, V. Path integral simulations of mixed para-D<sub>2</sub> and ortho-D<sub>2</sub> clusters: The orientational effects. *J. Chem. Phys.* **1994**, *100*, 7610–7629.
- (66) Hirschfelder, J. O.; Curtiss, C. F.; Bird, R. B. *Molecular theory of gases and liquids*, 1st ed.; John Wiley: New York, 1964.
- (67) Cracknell, R. F. Molecular Simulation of hydrogen adsorption in graphitic nanofibres. *Phys. Chem. Chem. Phys.* **2001**, *3*, 2091–2097.
- (68) Alavi, S.; Ripmeester, J.; Klug, D. Molecular-dynamics study of structure II hydrogen clathrates. *J. Chem. Phys.* **2005**, *123*, 024507.
- (69) Abascal, J. L.; Vega, C. A general purpose model for the condensed phases of water: TIP4P/2005. *J. Chem. Phys.* **2005**, *123*, 234505.
- (70) Garcia-Ratés, M.; de Hemptinne, J.-C.; Avalos, J. B.; Nieto-Draghi, C. Molecular Modeling of Diffusion Coefficient and Ionic Conductivity of CO<sub>2</sub> in Aqueous Ionic Solutions. *J. Phys. Chem. B* **2012**, *116*, 2787–2800.
- (71) Aimoli, C. G.; Maginn, E. J.; Abreu, C. R. Transport properties of carbon dioxide and methane from molecular dynamics simulations. *J. Chem. Phys.* **2014**, *141*, 134101.
- (72) Zhong, H.; Lai, S.; Wang, J.; Qiu, W.; Ludemann, H.-D.; Chen, L. Molecular dynamics simulation of transport and structural properties of CO<sub>2</sub> using different molecular models. *J. Chem. Eng. Data* **2015**, *60*, 2188–2196.
- (73) Jiang, H.; Economou, I. G.; Panagiotopoulos, A. Z. Molecular modeling of thermodynamic and transport properties for CO<sub>2</sub> and aqueous brines. *Acc. Chem. Res.* **2017**, *50*, 751–758.
- (74) Lopez-Lazaro, C.; Bachaud, P.; Moretti, I.; Ferrando, N. Predicting the phase behavior of hydrogen in NaCl brines by Molecular Simulation for geological applications. *BSGF-Earth Sci. Bulletin* **2019**, *190*, 7.
- (75) Liu, Y.; Panagiotopoulos, A. Z.; Debenedetti, P. G. Monte Carlo simulations of high-pressure phase equilibria of CO<sub>2</sub>-H<sub>2</sub>O mixtures. *J. Phys. Chem. B* **2011**, *115*, 6629–6635.
- (76) Liu, Y.; Lafitte, T.; Panagiotopoulos, A. Z.; Debenedetti, P. G. Simulations of vapor-liquid phase equilibrium and interfacial tension in the CO<sub>2</sub>-H<sub>2</sub>O-NaCl system. *AIChE J.* **2013**, *59*, 3514–3522.
- (77) Habibi, P.; Rahbari, A.; Blazquez, S.; Vega, C.; Dey, P.; Vlugt, T. J. H.; Moultsos, O. A. A New Force Field for OH- for Computing Thermodynamic and Transport Properties of H<sub>2</sub> and O<sub>2</sub> in Aqueous NaOH and KOH Solutions. *J. Phys. Chem. B* **2022**, *126*, 9376–9387.
- (78) Rahbari, A.; Hens, R.; Ramdin, M.; Moultsos, O. A.; Dubbeldam, D.; Vlugt, T. J. H. Recent advances in the Continuous Fractional Component Monte Carlo methodology. *Mol. Simul.* **2021**, *47*, 804–823.
- (79) Shi, W.; Maginn, E. J. Continuous Fractional Component Monte Carlo: an adaptive biasing method for open system atomistic simulations. *J. Chem. Theory Comput.* **2007**, *3*, 1451–1463.
- (80) Shi, W.; Maginn, E. J. Improvement in molecule exchange efficiency in Gibbs ensemble Monte Carlo: Development and implementation of the Continuous Fractional Component move. *J. Comput. Chem.* **2008**, *29*, 2520–2530.
- (81) Zeron, I. M.; Abascal, J. L. F.; Vega, C. A force field of Li<sup>+</sup>, Na<sup>+</sup>, K<sup>+</sup>, Mg<sup>2+</sup>, Ca<sup>2+</sup>, Cl<sup>-</sup>, and SO<sub>4</sub><sup>2-</sup> in aqueous solution based on the TIP4P/2005 water model and scaled charges for the ions. *J. Chem. Phys.* **2019**, *151*, 104501.
- (82) Blazquez, S.; Conde, M. M.; Vega, C. Unpublished. 2023.
- (83) Vega, C.; Abascal, J. L. Simulating water with rigid non-polarizable models: a general perspective. *Phys. Chem. Chem. Phys.* **2011**, *13*, 19663–19688.
- (84) Tsimpanogiannis, I. N.; Moultsos, O. A.; Franco, L. F.; Spera, M. B. M.; Erdös, M.; Economou, I. G. Self-diffusion coefficient of bulk and confined water: a critical review of classical Molecular Simulation studies. *Mol. Simul.* **2019**, *45*, 425–453.
- (85) González, M. A.; Abascal, J. L. The shear viscosity of rigid water models. *J. Chem. Phys.* **2010**, *132*, 096101.
- (86) Moultsos, O. A.; Tsimpanogiannis, I. N.; Panagiotopoulos, A. Z.; Economou, I. G. Atomistic molecular dynamics simulations of CO<sub>2</sub> diffusivity in H<sub>2</sub>O for a wide range of temperatures and pressures. *J. Phys. Chem. B* **2014**, *118*, 5532–5541.
- (87) Sakamaki, R.; Sum, A. K.; Narumi, T.; Ohmura, R.; Yasuoka, K. Thermodynamic properties of methane/water interface predicted by molecular dynamics simulations. *J. Chem. Phys.* **2011**, *134*, 144702.
- (88) Vega, C.; de Miguel, E. Surface tension of the most popular models of water by using the test-area simulation method. *J. Chem. Phys.* **2007**, *126*, 154707.
- (89) Döpke, M. F.; Moultsos, O. A.; Hartkamp, R. On the transferability of ion parameters to the TIP4P/2005 water model using molecular dynamics simulations. *J. Chem. Phys.* **2020**, *152*, 024501.
- (90) Deeg, K. S.; Gutiérrez-Sevillano, J. J.; Bueno-Pérez, R.; Parra, J. B.; Ania, C. O.; Doblaré, M.; Calero, S. Insights on the Molecular Mechanisms of Hydrogen Adsorption in Zeolites. *J. Phys. Chem. C* **2013**, *117*, 14374–14380.

- (91) Sesé, L. M. Study of the Feynman-Hibbs effective potential against the path-integral formalism for Monte Carlo simulations of quantum many-body Lennard-Jones systems. *Mol. Phys.* **1994**, *81*, 1297–1312.
- (92) Sesé, L. M. Feynman-Hibbs potentials and path integrals for quantum Lennard-Jones systems: Theory and Monte Carlo simulations. *Mol. Phys.* **1995**, *85*, 931–947.
- (93) Rahbari, A.; Brenkman, J.; Hens, R.; Ramdin, M.; van den Broeke, L. J. P.; Schoon, R.; Henkes, R.; Moultsos, O. A.; Vlugt, T. J. H. Solubility of water in hydrogen at high pressures: A Molecular Simulation study. *J. Chem. Eng. Data* **2019**, *64*, 4103–4115.
- (94) Plimpton, S. Fast Parallel Algorithms for Short-Range Molecular Dynamics. *J. Comput. Phys.* **1995**, *117*, 1–19.
- (95) Ryckaert, J. P.; Ciccotti, G.; Berendsen, H. J. Numerical integration of the cartesian equations of motion of a system with constraints: molecular dynamics of n-alkanes. *J. Comput. Phys.* **1977**, *23*, 327–341.
- (96) Allen, M. P.; Tildesley, D. J. *Computer simulation of liquids*; Oxford University Press, 2017.
- (97) Frenkel, D.; Smit, B. *Understanding Molecular Simulation: from algorithms to applications*, 2nd ed.; Elsevier: San Diego, 2002.
- (98) Hockney, R.; Eastwood, J. *Computer Simulation Using Particles*, 1st ed.; CRC Press: New York, 1988.
- (99) Plimpton, S. *LAMMPS Documentation (15 Sep 2022 version)*. <https://docs.lammps.org/Manual.html> (accessed: 26/10/2022).
- (100) Martinez, L.; Andrade, R.; Birgin, E. G.; Martínez, J. M. PACKMOL: A package for building initial configurations for molecular dynamics simulations. *J. Comput. Chem.* **2009**, *30*, 2157–2164.
- (101) Isele-Holder, R. E.; Mitchell, W.; Ismail, A. E. Development and application of a particle-particle particle-mesh Ewald method for dispersion interactions. *J. Chem. Phys.* **2012**, *137*, 174107.
- (102) Salehi, H. S.; Moultsos, O. A.; Vlugt, T. J. H. Interfacial Properties of Hydrophobic Deep Eutectic Solvents with Water. *J. Phys. Chem. B* **2021**, *125*, 12303–12314.
- (103) Rowlinson, J. S.; Widom, B. *Molecular theory of capillarity*, 1st ed.; Courier Corporation: Oxford, 1982.
- (104) Jamali, S. H.; Wolff, L.; Becker, T. M.; de Groen, M.; Ramdin, M.; Hartkamp, R.; Bardow, A.; Vlugt, T. J. H.; Moultsos, O. A. OCTP: A Tool for On-the-Fly Calculation of Transport Properties of Fluids with the Order-n Algorithm in LAMMPS. *J. Chem. Inf. Model.* **2019**, *59*, 1290–1294.
- (105) Dubbeldam, D.; Ford, D. C.; Ellis, D. E.; Snurr, R. Q. A new perspective on the order-n algorithm for computing correlation functions. *Mol. Simul.* **2009**, *35*, 1084–1097.
- (106) Yeh, I.-C.; Hummer, G. System-size dependence of diffusion coefficients and viscosities from molecular dynamics simulations with periodic boundary conditions. *J. Phys. Chem. B* **2004**, *108*, 15873–15879.
- (107) Celebi, A. T.; Jamali, S. H.; Bardow, A.; Vlugt, T. J. H.; Moultsos, O. A. Finite-size effects of diffusion coefficients computed from molecular dynamics: a review of what we have learned so far. *Mol. Simul.* **2021**, *47*, 831–845.
- (108) Jamali, S. H.; Bardow, A.; Vlugt, T. J. H.; Moultsos, O. A. Generalized form for finite-size corrections in mutual diffusion coefficients of multicomponent mixtures obtained from equilibrium molecular dynamics simulation. *J. Chem. Theory Comput.* **2020**, *16*, 3799–3806.
- (109) Moultsos, O. A.; Zhang, Y.; Tsimpanogiannis, I. N.; Economou, I. G.; Maginn, E. J. System-size corrections for self-diffusion coefficients calculated from molecular dynamics simulations: The case of CO<sub>2</sub>, n-alkanes, and poly (ethylene glycol) dimethyl ethers. *J. Chem. Phys.* **2016**, *145*, 074109.
- (110) Jamali, S. H.; Hartkamp, R.; Bardas, C.; Sohl, J.; Vlugt, T. J. H.; Moultsos, O. A. Shear viscosity computed from the finite-size effects of self-diffusivity in equilibrium molecular dynamics. *J. Chem. Theory Comput.* **2018**, *14*, 5959–5968.
- (111) Jamali, S. H.; Wolff, L.; Becker, T. M.; Bardow, A.; Vlugt, T. J. H.; Moultsos, O. A. Finite-size effects of binary mutual diffusion coefficients from molecular dynamics. *J. Chem. Theory Comput.* **2018**, *14*, 2667–2677.
- (112) Hens, R.; Rahbari, A.; Caro-Ortiz, S.; Dawass, N.; Erdos, M.; Poursaeidesfahani, A.; Salehi, H. S.; Celebi, A. T.; Ramdin, M.; Moultsos, O. A.; Dubbeldam, D.; Vlugt, T. J. H. Brick-CFCMC: Open Source Software for Monte Carlo Simulations of Phase and Reaction Equilibria Using the Continuous Fractional Component Method. *J. Chem. Inf. Model.* **2020**, *60*, 2678–2682.
- (113) Polat, H. M.; Salehi, H. S.; Hens, R.; Wasik, D. O.; Rahbari, A.; de Meyer, F.; Houriez, C.; Coquelet, C.; Calero, S.; Dubbeldam, D.; Moultsos, O. A.; Vlugt, T. J. H. New Features of the Open Source Monte Carlo Software Brick-CFCMC: Thermodynamic Integration and Hybrid Trial Moves. *J. Chem. Inf. Model.* **2021**, *61*, 3752–3757.
- (114) Poursaeidesfahani, A.; Hens, R.; Rahbari, A.; Ramdin, M.; Dubbeldam, D.; Vlugt, T. J. H. Efficient application of Continuous Fractional Component Monte Carlo in the reaction ensemble. *J. Chem. Theory Comput.* **2017**, *13*, 4452–4466.
- (115) Rahbari, A.; Hens, R.; Dubbeldam, D.; Vlugt, T. J. H. Improving the accuracy of computing chemical potentials in CFCMC simulations. *Mol. Phys.* **2019**, *117*, 3493–3508.
- (116) Rahbari, A.; Hens, R.; Jamali, S.; Ramdin, M.; Dubbeldam, D.; Vlugt, T. J. H. Effect of truncating electrostatic interactions on predicting thermodynamic properties of water-methanol systems. *Mol. Simul.* **2019**, *45*, 336–350.
- (117) Wang, F.; Landau, D. P. Efficient multiple-range random walk algorithm to calculate the density of states. *Phys. Rev. Lett.* **2001**, *86*, 2050.
- (118) Wang, F.; Landau, D. P. Determining the density of states for classical statistical models: A random walk algorithm to produce a flat histogram. *Phys. Rev. E* **2001**, *64*, 056101.
- (119) Salehi, H. S.; Hens, R.; Moultsos, O. A.; Vlugt, T. J. H. Computation of gas solubilities in choline chloride urea and choline chloride ethylene glycol deep eutectic solvents using Monte Carlo simulations. *J. Mol. Liq.* **2020**, *316*, 113729.
- (120) Widom, B. Potential-distribution theory and the statistical mechanics of fluids. *J. Phys. Chem.* **1982**, *86*, 869–872.
- (121) Widom, B. Some Topics in the Theory of Fluids. *J. Chem. Phys.* **1963**, *39*, 2808–2812.
- (122) Rahbari, A.; Hens, R.; Nikolaidis, I. K.; Poursaeidesfahani, A.; Ramdin, M.; Economou, I. G.; Moultsos, O. A.; Dubbeldam, D.; Vlugt, T. J. H. Computation of partial molar properties using continuous fractional component Monte Carlo. *Mol. Phys.* **2018**, *116*, 3331–3344.
- (123) Georgiadis, A.; Maitland, G.; Trusler, J. M.; Bismarck, A. Interfacial tension measurements of the (H<sub>2</sub>O+CO<sub>2</sub>) system at elevated pressures and temperatures. *J. Chem. Eng. Data* **2010**, *55*, 4168–4175.
- (124) Bachu, S.; Bennion, D. B. Interfacial tension between CO<sub>2</sub>, freshwater, and brine in the range of pressure from (2 to 27) MPa, temperature from (20 to 125) °C, and water salinity from (0 to 334 000) mg·L<sup>-1</sup>. *J. Chem. Eng. Data* **2009**, *54*, 765–775.
- (125) Hebach, A.; Oberhof, A.; Dahmen, N.; Kögel, A.; Ederer, H.; Dinjus, E. Interfacial tension at elevated pressures measurements and correlations in the water+ carbon dioxide system. *J. Chem. Eng. Data* **2002**, *47*, 1540–1546.
- (126) Ren, Q.-Y.; Chen, G.-J.; Yan, W.; Guo, T.-M. Interfacial tension of (CO<sub>2</sub>+CH<sub>4</sub>)<sub>n</sub> water from 298 to 373 K and pressures up to 30 MPa. *J. Chem. Eng. Data* **2000**, *45*, 610–612.
- (127) Naeiji, P.; Woo, T. K.; Alavi, S.; Ohmura, R. Molecular dynamics simulations of interfacial properties of the CO<sub>2</sub>-water and CO<sub>2</sub>-CH<sub>4</sub>-water systems. *J. Chem. Phys.* **2020**, *153*, 044701.
- (128) Li, X.; Boek, E.; Maitland, G. C.; Trusler, J. P. M. Interfacial Tension of (Brines+CO<sub>2</sub>):(0.864 NaCl+0.136 KCl) at Temperatures between (298 and 448) K, Pressures between (2 and 50) MPa, and Total Molalities of (1 to 5) mol·kg<sup>-1</sup>. *J. Chem. Eng. Data* **2012**, *57*, 1078–1088.
- (129) Aggelopoulos, C. A.; Robin, M.; Vizika, O. Interfacial tension between CO<sub>2</sub> and brine (NaCl+CaCl<sub>2</sub>) at elevated pressures and

- temperatures: The additive effect of different salts. *Adv. Water Resour.* **2011**, *34*, 505–511.
- (130) Jerauld, G. R.; Kazemi, A. An improved simple correlation for accurate estimation of CO<sub>2</sub>-Brine interfacial tension at reservoir conditions. *J. Pet. Sci. Eng.* **2022**, *208*, 109537.
- (131) Manciu, M.; Ruckenstein, E. Specific ion effects via ion hydration: I. Surface tension. *Adv. Colloid Interface Sci.* **2003**, *105*, 63–101.
- (132) Marcus, Y. Effect of ions on the structure of water: Structure making and breaking. *Chem. Rev.* **2009**, *109*, 1346–1370.
- (133) Pegram, L. M.; Record, M. T. Hofmeister salt effects on surface tension arise from partitioning of anions and cations between bulk water and the air-water interface. *J. Phys. Chem. B* **2007**, *111*, 5411–5417.
- (134) Levin, Y.; dos Santos, A. P.; Diehl, A. Ions at the air-water interface: An end to a hundred-year-old mystery? *Phys. Rev. Lett.* **2009**, *103*, 257802.
- (135) Weisenberger, S.; Schumpe, A. Estimation of gas solubilities in salt solutions at temperatures from 273 to 363 K. *AIChE J.* **1996**, *42*, 298–300.
- (136) Laliberté, M. Model for calculating the viscosity of aqueous solutions. *J. Chem. Eng. Data* **2007**, *52*, 321–335.
- (137) Laliberté, M.; Cooper, W. E. Model for calculating the density of aqueous electrolyte solutions. *J. Chem. Eng. Data* **2004**, *49*, 1141–1151.
- (138) Tsimpanogiannis, I. N.; Moulton, O. A. Is Stokes-Einstein relation valid for the description of intra-diffusivity of hydrogen and oxygen in liquid water? *Fluid Phase Equilib.* **2022**, *563*, 113568.
- (139) Cussler, E. L. *Diffusion Coefficients and Diffusion of Interacting Species*, 2nd ed.; Cambridge University Press: Cambridge, 2009.
- (140) Taylor, R.; Krishna, R. *Multicomponent mass transfer*, 1st ed.; John Wiley & Sons, 1993; Vol. 2.
- (141) Krishna, R.; Wesselingh, J. The Maxwell-Stefan approach to mass transfer. *Chem. Eng. Sci.* **1997**, *52*, 861–911.
- (142) Wiebe, R.; Gaddy, V. L. The Solubility of Hydrogen in Water at 0, 50, 75 and 100° from 25 to 1000 atm. *J. Am. Chem. Soc.* **1934**, *56*, 76–79.
- (143) Wiebe, R.; Gaddy, V.; Heins, C. Solubility of Hydrogen in Water at 25° C. from 25 to 1000 atm. *Ind. Eng. Chem.* **1932**, *24*, 823–825.
- (144) Kling, G.; Maurer, G. The solubility of hydrogen in water and in 2-aminoethanol at temperatures between 323 and 423 K and pressures up to 16 MPa. *J. Chem. Thermodyn.* **1991**, *23*, 531–541.
- (145) Choudhary, V. R.; Parande, M. G.; Brahme, P. H. Simple apparatus for measuring solubility of gases at high pressures. *Ind. Eng. Chem. Fundam.* **1982**, *21*, 472–474.
- (146) Chandrasekhar, J.; Spellmeyer, D. C.; Jorgensen, W. L. Energy component analysis for dilute aqueous solutions of lithium (1+), sodium (1+), fluoride (1-), and chloride (1-) ions. *J. Am. Chem. Soc.* **1984**, *106*, 903–910.
- (147) Darkrim, F.; Vermesse, J.; Malbrunot, P.; Levesque, D. Monte Carlo simulations of nitrogen and hydrogen physisorption at high pressures and room temperature. Comparison with experiments. *J. Chem. Phys.* **1999**, *110*, 4020–4027.
- (148) Zhu, Z.; Cao, Y.; Zheng, Z.; Chen, D. An Accurate Model for Estimating H<sub>2</sub> Solubility in Pure Water and Aqueous NaCl Solutions. *Energies* **2022**, *15*, 5021.

# Supporting Information: Interfacial tensions, solubilities, and transport properties of the $\text{H}_2/\text{H}_2\text{O}/\text{NaCl}$ system: A molecular simulation study

W. A. van Rooijen,<sup>†,§</sup> P. Habibi,<sup>‡,¶,§</sup> K. Xu,<sup>¶</sup> P. Dey,<sup>¶</sup> T. J. H. Vlugt,<sup>‡</sup> H. Hajibeygi,<sup>†</sup> and O. A. Moulton<sup>\*,‡</sup>

<sup>†</sup>*Reservoir Engineering, Geoscience and Engineering Department, Faculty of Civil Engineering and Geosciences, Delft University of Technology, Stevinweg 1, 2628CN, Delft, The Netherlands*

<sup>‡</sup>*Engineering Thermodynamics, Process and Energy Department, Faculty of Mechanical, Maritime and Materials Engineering, Delft University of Technology, Leeghwaterstraat 39, 2628CB, Delft, The Netherlands*

<sup>¶</sup>*Department of Materials Science and Engineering, Faculty of Mechanical, Maritime and Materials Engineering, Delft University of Technology, Mekelweg 2, 2628CD, Delft, The Netherlands*

<sup>§</sup>*These authors contributed equally*

E-mail: o.moulton@tudelft.nl

Solubilities of H<sub>2</sub> in pure water (Table S1); Force field parameters (Tables S2 - S5); Additional info MD and CFCMC simulations (Tables S6 - S8); Raw data MD simulations for Interfacial Tensions (Table S9); Density and viscosity data (Table S10); Raw data MD simulations for self-diffusivities (Tables S11 - S12); Raw data CFCMC simulations (Table S13); Solubilities of H<sub>2</sub> in pure water (Figure S1); Density profile of Na<sup>+</sup> and Cl<sup>-</sup> of a MD simulation to calculate interfacial tensions (Figure S2); Solubilities of H<sub>2</sub> in aqueous NaCl solution at H<sub>2</sub> partial pressures of 1-100 bar (Figure S3); Densities of NaCl solutions (Figure S4); Viscosities of NaCl solutions (Figure S5).

Table S1: Computed solubilities of  $\text{H}_2$  at a  $\text{H}_2$  partial pressure of 1 bar in pure water using the TIP4P/2005<sup>1</sup>  $\text{H}_2\text{O}$  force field in combination with the Marx<sup>2</sup>  $\text{H}_2$  force field and the Vrabec<sup>3</sup> force field as a function of temperature  $T$ .  $T$  is in unit of K,  $x_{\text{H}_2}$  and  $\sigma_{x_{\text{H}_2}}$  are reported with multiplication factors of  $10^{-5}$ .  $\sigma_{x_{\text{H}_2}}$  is the uncertainty of  $x_{\text{H}_2}$ . The last column lists the calculated solubilities using the experimental correlation provided by Torín-Ollarves and Trusler<sup>4</sup>

$T$	Marx <sup>2</sup>		Vrabec <sup>3</sup>		Experimental <sup>4</sup>
	$x_{\text{H}_2}$	$\sigma_{x_{\text{H}_2}}$	$x_{\text{H}_2}$	$\sigma_{x_{\text{H}_2}}$	$x_{\text{H}_2}$
298	1.30	0.03	0.66	0.01	1.39
323	1.19	0.02	0.68	0.02	1.29
333	-	-	0.69	0.01	1.29
343	1.20	0.02	0.72	0.03	1.32
353	-	-	0.75	0.01	1.36
363	1.28	0.02	-	-	1.42

Table S2: Parameters for the TIP4P/2005<sup>1</sup> water force field.  $\sigma$  and  $\epsilon$  are the Lennard-Jones parameters,  $q$  is the atomic partial charge, and  $l$  is the bond length.  $\sigma$  and  $l$  are in units of Å,  $\epsilon$  is in units of kJ/mol, and  $q$  is in units of the elementary charge e. In the TIP4P/2005<sup>1</sup> force field, the charge on O is on a massless site M.

$\text{H} - \widehat{\text{O}} - \text{H}$ (°)	104.52
$l_{\text{O}-\text{H}}$	0.9572
$l_{\text{O}-\text{M}}$	0.1546
$\sigma_{\text{OO}}$	3.1589
$\sigma_{\text{HH}}$	0
$\epsilon_{\text{OO}}$	0.774908
$\epsilon_{\text{HH}}$	0
$q_{\text{O}}$	0
$q_{\text{M}}$	-1.1128
$q_{\text{H}}$	0.5564

Table S3: Parameters for the single-site Vrabec<sup>3</sup> Hydrogen force field.  $\sigma$  and  $\epsilon$  are the Lennard-Jones parameters.  $\sigma$  is in units of Å and  $\epsilon$  is in units of kJ/mol.

$\sigma_{\text{HH}}$	3.0366
$\epsilon_{\text{HH}}$	0.214846

Table S4: Parameters for the three-site Marx<sup>2</sup> Hydrogen force field.  $\sigma$  and  $\epsilon$  are the Lennard-Jones parameters,  $q$  is the atomic partial charge, dummy site  $L$  is the geometric center of mass, and  $l$  is the bond length.  $\sigma$  and  $l$  are in units of Å,  $\epsilon$  is in units of kJ/mol, and  $q$  is in units of the elementary charge e.

$\sigma_{LL}$	2.958
$\epsilon_{LL}$	0.305141
$q_H$	0.468
$q_L$	-0.936
$l_{H-H}$	0.74

Table S5: Parameters for the Madrid-Transport<sup>5,6</sup> and Madrid-2019<sup>7</sup> force fields.  $\sigma$  and  $\epsilon$  are the Lennard-Jones parameters and  $q$  is the atomic partial charge.  $\sigma$  is units of Å,  $\epsilon$  is in units of kJ/mol, and  $q$  is in units of the elementary charge e.

	Madrid-Transport	Madrid-2019
$\sigma_{Na^+Na^+}$	2.21737	2.21737
$\sigma_{Na^+Cl^-}$	2.58012	3.00512
$\sigma_{Cl^-Cl^-}$	4.69906	4.69906
$\sigma_{Na^+O_w}$	2.38725	2.60838
$\sigma_{Cl^-O_w}$	4.07631	4.23867
$\epsilon_{Na^+Na^+}$	1.472356	1.472356
$\epsilon_{Na^+Cl^-}$	1.438894	1.438894
$\epsilon_{Cl^-Cl^-}$	0.076923	0.076923
$\epsilon_{Na^+O_w}$	0.793388	0.793388
$\epsilon_{Cl^-O_w}$	0.061983	0.061983
$q_{Na^+}$	0.75	0.85
$q_{Cl^-}$	-0.75	-0.85

Table S6: The numbers of H<sub>2</sub>, H<sub>2</sub>O molecules, and Na<sup>+</sup> and Cl<sup>-</sup> ions  $N_{\text{H}_2}$ ,  $N_{\text{H}_2\text{O}}$ ,  $N_{\text{Na}^+/\text{Cl}^-}$ , used in the MD simulations to compute interfacial tensions for a wide range of pressures  $P$ , temperatures  $T$ , and NaCl molalities  $m_{\text{NaCl}}$ . The different columns represent different NaCl molalities. The last column reports the average simulation cell sizes  $L_x$ ,  $L_y$  and  $L_z$  for a molarity of 1.01 mol NaCl/kg H<sub>2</sub>O.  $T$  is in units of K,  $P$  is in units of bar,  $m_{\text{NaCl}}$  is in units of mol NaCl/kg H<sub>2</sub>O, and  $L$  is in Å.

$T$	$m_{\text{NaCl}}$	$N_{\text{H}_2}$	$N_{\text{H}_2\text{O}}$	$N_{\text{Na}^+/\text{Cl}^-}$	$L_x \times L_y \times L_z$												
		0.00	0.00	0.00	1.01	1.01	1.01	3.00	3.00	3.00	5.00	5.00	5.00	5.00	5.00	5.00	1.01
298	1	64	2088	0	64	2088	38	64	2090	113	64	2090	188	39	39	101	
	10	320	2088	0	320	2088	38	320	2090	113	320	2090	188	39	39	430	
	100	640	2088	0	640	2088	38	640	2090	113	640	2090	188	39	39	203	
	200	640	2088	0	640	2088	38	640	2090	113	640	2090	188	39	39	139	
400	400	640	2088	0	640	2088	38	640	2090	113	640	2090	188	39	39	96	
	600	640	2088	0	640	2088	38	640	2090	113	640	2090	188	39	39	83	
	1	64	2088	0	64	2088	38	64	2090	113	64	2090	188	39	39	118	
	10	320	2088	0	320	2088	38	320	2090	113	320	2090	188	39	39	468	
400	100	640	2088	0	640	2088	38	640	2090	113	640	2090	188	39	39	216	
	138	-	-	-	640	2088	38	-	-	-	-	-	-	39	39	179	
	323	400	640	2088	0	640	2088	38	640	2090	113	640	2090	188	39	39	147
	276	-	-	-	640	2088	38	-	-	-	-	-	-	39	39	124	
400	400	640	2088	0	640	2088	38	640	2090	113	640	2090	188	39	39	100	
	600	640	2088	0	640	2088	38	640	2090	113	640	2090	188	39	39	86	
	1	64	2088	0	64	2088	38	64	2090	113	64	2090	188	39	39	121	
	10	320	2088	0	320	2088	38	320	2090	113	320	2090	188	39	39	508	
343	100	640	2088	0	640	2088	38	640	2090	113	640	2090	188	39	39	228	
	200	640	2088	0	640	2088	38	640	2090	113	640	2090	188	39	39	152	
	400	640	2088	0	640	2088	38	640	2090	113	640	2090	188	39	39	103	
	600	640	2088	0	640	2088	38	640	2090	113	640	2090	188	39	39	88	
373	1	64	2088	0	64	2088	38	64	2090	113	64	2090	188	39	39	114	
	10	320	2088	0	320	2088	38	320	2090	113	320	2090	188	39	39	629	
	100	640	2088	0	640	2088	38	640	2090	113	640	2090	188	39	39	246	
	138	-	-	-	640	2088	38	-	-	-	-	-	-	39	39	200	
423	200	640	2088	0	640	2088	38	640	2090	113	640	2090	188	39	39	162	
	400	640	2088	0	640	2088	38	640	2090	113	640	2090	188	39	39	136	
	600	640	2088	0	640	2088	38	640	2090	113	640	2090	188	39	39	92	
	100	640	2088	0	640	2088	38	640	2090	113	640	2090	188	39	39	281	
423	200	640	2088	0	640	2088	38	640	2090	113	640	2090	188	39	39	178	
	400	640	2088	0	640	2088	38	640	2090	113	640	2090	188	39	39	121	
	600	640	2088	0	640	2088	38	640	2090	113	640	2090	188	39	39	99	
	200	640	2088	0	640	2088	38	640	2090	113	640	2090	188	39	39	228	
523	400	640	2088	0	640	2088	38	640	2090	113	640	2090	188	39	39	145	
	600	640	2088	0	640	2088	38	640	2090	113	640	2090	188	39	39	116	

Table S7: The numbers of molecules or ions  $N$  used in the MD simulations to compute self-diffusivities.  $m_{\text{NaCl}}$  is in units of mol NaCl/kg water. For each molality, the same numbers of molecules and ions are used for all temperatures and pressures

$m_{\text{NaCl}}$	$N_{\text{H}_2}$	$N_{\text{H}_2\text{O}}$	$N_{\text{Na}^+}$	$N_{\text{Cl}^-}$
0	2	700	0	0
1.03	2	700	13	13
3.01	2	700	38	38
5.00	2	700	63	63
6.03	2	700	76	76

Table S8: The numbers of molecules or ions  $N$  used in the CFCMC simulations.  $m_{\text{NaCl}}$  is in units of mol NaCl/kg water. For each molality, the same numbers of molecules and ions are used for all temperatures and pressures. In every simulation, a single fractional molecule of  $\text{H}_2$  used.

$m_{\text{NaCl}}$	$N_{\text{H}_2\text{O}}$	$N_{\text{Na}^+}$	$N_{\text{Cl}^-}$
0	300	0	0
0.93	300	5	5
2.96	300	16	16
5.00	300	27	27
5.93	300	32	32

Table S9: The interfacial tensions  $\gamma$  of  $\text{H}_2$  in contact with aqueous NaCl solutions as computed using the NaCl Madrid-2019<sup>7</sup> force field, the TIP4P/2005<sup>1</sup> water force field, and the Vrabec<sup>3</sup> hydrogen force field.  $T$  is in units of K,  $P$  is in units of bar,  $m_{\text{NaCl}}$  is in units of mol NaCl/kg  $\text{H}_2\text{O}$ , and  $\gamma$  is in units of mN/m.  $\sigma_\gamma$  is the uncertainty of  $\gamma$ . Conditions at which simulations are not performed are denoted by -. Uncertainties in pressure and temperature are zero as these are imposed in the simulations (*NPT* ensemble).

		$\gamma$	$\sigma_\gamma$	$\gamma$	$\sigma_\gamma$	$\gamma$	$\sigma_\gamma$	$\gamma$	$\sigma_\gamma$
	$m_{\text{NaCl}}$	0.00		1.01		3.00		5.00	
$T$	$P$								
298	1	64.9	0.7	67	1	69	1	73	1
	10	66	1	68	2	70.3	0.8	72.8	0.4
	100	65	1	68	1	69	2	73	1
	200	65.1	0.7	66	2	68.4	0.8	71.3	0.9
	400	64.0	0.8	66.6	0.8	69	1	70	1
	600	65	1	66	1	68.4	0.6	72.0	0.7
323	1	62.3	0.9	63.5	0.7	66.5	0.8	70	1
	10	61.9	0.1	64.4	0.8	66.6	0.9	69.9	0.7
	100	61.5	0.9	63	1	66.3	0.6	68	2
	138	-	-	63.7	0.6	-	-	-	-
	400	61.6	0.6	62.9	0.8	65.0	0.8	68	1
	276	-	-	63	1	-	-	-	-
	400	61.0	0.3	63	1	65.4	0.8	69	2
	600	61.0	0.5	63	1	65.0	0.9	70	1
343	1	58.6	0.6	60.0	0.8	63.2	0.3	66.1	0.5
	10	58.9	0.5	60.9	0.9	64.1	0.4	64.7	0.9
	100	58.8	0.4	60.7	0.8	62.8	0.8	66	1
	200	58	1	59.5	0.5	63	1	64.1	0.9
	400	58	1	60.4	0.8	63.1	0.5	65	1
	600	59.3	0.6	59.9	0.9	63	1	67.6	0.7
373	1	53.2	0.5	55.6	0.6	58.4	0.8	61	1
	10	54.3	0.2	55	1	57.8	0.4	61.0	0.9
	100	54.3	0.4	55.8	0.9	57.4	0.6	61.6	0.4
	138	-	-	56	1	-	-	-	-
	200	53.7	0.4	55.1	0.4	58.6	0.4	61	1
	276	-	-	56	1	-	-	-	-
	400	53.1	0.2	55.2	0.4	58.5	0.4	60.6	0.5
	600	54.1	0.6	55.4	0.4	58.1	0.6	61.2	0.4
423	100	44.0	0.8	46.3	0.5	49.6	0.9	52.1	0.7
	200	45.2	0.9	47.3	0.4	50.1	0.5	53.7	0.6
	400	45.2	0.5	47.6	0.6	50.3	0.7	53	1
	600	45.3	0.5	47.8	0.9	50.6	0.5	54	1
523	200	25	1	27.5	0.9	31.6	0.8	34.5	0.7
	400	25.4	0.4	27.2	0.4	32.0	0.1	35.6	0.7
	600	26.0	0.6	29.5	0.5	32.7	0.8	36	1

Table S10: The densities  $\rho$  and viscosities  $\eta$  of aqueous NaCl solutions as computed using the NaCl Madrid-2019<sup>7</sup> and Madrid-Transport<sup>5,6</sup> force fields, compared with a fit to experimental data for densities<sup>8</sup> and viscosities.<sup>9</sup> The TIP4P/2005<sup>1</sup> H<sub>2</sub>O force field and the Vrabec<sup>3</sup> H<sub>2</sub> force field were used.  $T$  is in units of K,  $P$  is in units of bar,  $m_{\text{NaCl}}$  is in units of mol NaCl/kg H<sub>2</sub>O,  $\rho$  is in units of kg/m<sup>3</sup> and  $\eta$  is in units of mPa·s.  $\sigma_x$  is the uncertainty of quantity  $x$ .

		Madrid-2019 <sup>7</sup>				Madrid-Transport <sup>5,6</sup>				Experimental <sup>8,9</sup>	
$T$	$m_{\text{NaCl}}$	$\rho$	$\sigma_\rho$	$\eta$	$\sigma_\eta$	$\rho$	$\sigma_\rho$	$\eta$	$\sigma_\eta$	$\rho$	$\eta$
298	0.00	994	1	0.888	0.008	993.9	0.5	0.83	0.05	997.0	0.890
	0.93	1034.0	0.4	0.96	0.03	1032.4	0.4	0.969	0.003	1036.2	0.927
	2.96	1103.0	0.5	1.5	0.1	1100.8	0.4	1.22	0.05	1106.1	1.198
	5.00	1163.5	0.5	2.2	0.2	1162.1	0.6	1.5	0.1	1166.3	1.527
	5.93	1191.6	0.5	2.6	0.4	1192.3	0.4	1.8	0.2	1193.3	1.754
323	0.00	973.0	0.7	0.393	0.001	973.4	0.3	0.40	0.02	977.8	0.404
	0.93	1010.6	0.3	0.47	0.02	1010.2	0.1	0.50	0.05	1015.1	0.452
	2.93	1075.3	0.3	0.64	0.02	1076.8	0.3	0.57	0.06	1082.5	0.566
	5.00	1132.4	0.3	0.84	0.03	1136.8	0.3	0.72	0.04	1141.5	0.708
	5.93	1162.6	0.3	0.95	0.07	1165.9	0.4	0.78	0.05	1168.3	0.794

Table S11: Results of MD simulations to compute self-diffusivities of H<sub>2</sub> in aqueous NaCl solutions as computed using the NaCl Madrid-Transport<sup>5,6</sup> force field, the TIP4P/2005<sup>1</sup> H<sub>2</sub>O force field, and the Vrabec<sup>3</sup> H<sub>2</sub> force field. The densities  $\rho$ , viscosities  $\eta$ , and H<sub>2</sub> finite-size corrected<sup>10</sup> self-diffusion coefficients  $D_{\text{H}_2}$  for a wide range of temperatures  $T$ , pressures  $P$ , NaCl molalities  $m_{\text{NaCl}}$ , and corresponding molarities  $M_{\text{NaCl}}$ .  $T$  is in units of K,  $P$  is in units of bar,  $m_{\text{NaCl}}$  is in units of mol NaCl/kg water,  $M_{\text{NaCl}}$  is in units of mol NaCl/L solution,  $\rho$  is in units of kg/m<sup>3</sup>,  $\eta$  is in units of mPa·s, and  $D$  is in units of 10<sup>-9</sup> m<sup>2</sup>/s.  $\sigma_x$  is the uncertainty of quantity  $x$ . Uncertainties in pressure and temperature are zero as these are imposed in the simulations (*NPT* ensemble).

$T$	$P$	$m_{\text{NaCl}}$	$M_{\text{NaCl}}$	$\sigma_M$	$\rho$	$\sigma_\rho$	$\eta$	$\sigma_\eta$	$D_{\text{H}_2}$	$\sigma_{D_{\text{H}_2}}$
298	1	0	0	0	993.9	0.5	0.82	0.05	4.4	0.6
298	1	1.03	1.0030	0.0004	1032.4	0.4	0.969	0.003	3.7	0.6
298	1	3.01	2.820	0.001	1100.8	0.4	1.22	0.05	3.2	0.1
298	1	5.00	4.492	0.002	1162.1	0.6	1.51	0.13	2.8	0.2
298	1	6.03	5.312	0.002	1192.3	0.4	1.81	0.16	2.5	0.1
298	10	0	0	0	994.6	0.4	0.85	0.02	4.6	0.2
298	10	1.03	1.0040	0.0002	1032.7	0.2	0.96	0.03	3.9	0.6
298	10	3.01	2.820	0.001	1100.8	0.5	1.24	0.06	3.0	0.3
298	10	5.00	4.492	0.002	1162.1	0.4	1.6	0.2	2.7	0.2

**Table S11 continued from previous page**

<i>T</i>	<i>P</i>	<i>m</i> <sub>NaCl</sub>	<i>M</i> <sub>NaCl</sub>	$\sigma_m$	$\rho$	$\sigma_\rho$	$\eta$	$\sigma_\eta$	<i>D</i> <sub>H<sub>2</sub></sub>	$\sigma_{D_{H_2}}$
298	10	6.03	5.313	0.002	1192.4	0.6	1.8	0.1	2.6	0.2
298	100	0	0	0	998.0	0.4	0.83	0.03	4.3	0.1
298	100	1.03	1.0080	0.0003	1036.9	0.3	1.0	0.1	3.9	0.4
298	100	3.01	2.8290	0.0004	1104.6	0.2	1.24	0.05	3.3	0.1
298	100	5.00	4.508	0.002	1166.0	0.5	1.6	0.1	2.9	0.2
298	100	6.03	5.329	0.002	1196.0	0.4	1.9	0.2	2.5	0.2
298	400	0.00	0.0	0.0	1011.2	0.4	0.83	0.04	4.3	0.2
298	400	1.03	1.0210	0.0003	1050.0	0.3	1.0	0.1	3.7	0.2
298	400	3.01	2.862	0.001	1117.3	0.5	1.3	0.1	2.9	0.2
298	400	5.00	4.556	0.001	1178.5	0.2	1.61	0.09	2.5	0.2
298	400	6.03	5.384	0.002	1208.4	0.4	1.77	0.08	2.2	0.2
298	1000	0	0	0	1036.4	0.3	0.9	0.1	3.9	0.3
298	1000	1.03	1.0440	0.0002	1073.9	0.2	0.92	0.07	3.4	0.2
298	1000	3.01	2.923	0.001	1141.2	0.4	1.3	0.2	2.1	0.4
298	1000	5.00	4.647	0.002	1202.2	0.5	1.47	0.03	2.4	0.3
298	1000	6.03	5.488	0.002	1231.6	0.4	1.8	0.1	2.1	0.1
343	1	0	0	0	973.4	0.3	0.40	0.02	9.4	0.4
343	1	1.03	0.9819	0.0001	1010.2	0.1	0.50	0.05	7.8	1.4
343	1	3.01	2.758	0.001	1076.8	0.3	0.57	0.06	6.8	0.7
343	1	5.00	4.395	0.001	1136.8	0.3	0.72	0.04	6	1
343	1	6.03	5.195	0.002	1165.9	0.4	0.78	0.05	6.0	0.1
343	10	0	0	0	973.2	0.3	0.40	0.02	8.9	0.6
343	10	1.03	0.9826	0.0002	1010.9	0.2	0.45	0.02	8.8	0.2
343	10	3.01	2.760	0.001	1077.5	0.5	0.56	0.02	7.5	0.2
343	10	5.00	4.396	0.001	1137.1	0.2	0.73	0.03	6.2	0.3
343	10	6.03	5.197	0.002	1166.3	0.4	0.74	0.06	6.0	0.4
343	100	0	0	0	977.6	0.2	0.39	0.01	9.2	0.5
343	100	1.03	0.9867	0.0003	1015.1	0.3	0.46	0.03	8	1
343	100	3.01	2.770	0.001	1081.3	0.4	0.57	0.02	7.1	0.6
343	100	5.00	4.411	0.001	1140.9	0.2	0.71	0.07	6.3	0.4

**Table S11 continued from previous page**

$T$	$P$	$m_{\text{NaCl}}$	$M_{\text{NaCl}}$	$\sigma_m$	$\rho$	$\sigma_\rho$	$\eta$	$\sigma_\eta$	$D_{\text{H}_2}$	$\sigma_{D_{\text{H}_2}}$
343	100	6.03	5.213	0.001	1170.0	0.3	0.75	0.05	5.9	0.2
343	400	0	0	0	991.0	0.2	0.41	0.01	8.7	0.3
343	400	1.031	0.9995	0.0002	1028.3	0.2	0.46	0.03	8.2	0.2
343	400	3.01	2.803	0.001	1094.5	0.3	0.57	0.02	7.0	0.5
343	400	5.00	4.461	0.001	1154.0	0.2	0.71	0.06	5.4	0.5
343	400	6.03	5.271	0.002	1182.9	0.4	0.80	0.04	5.2	0.7
343	1000	0	0	0	1015.2	0.2	0.42	0.02	7.9	0.3
343	1000	1.031	1.0230	0.0001	1052.3	0.1	0.50	0.05	7.1	0.2
343	1000	3.01	2.864	0.001	1118.3	0.2	0.59	0.02	6.1	0.5
343	1000	5.00	4.555	0.002	1178.2	0.5	0.73	0.04	5.9	0.9
343	1000	6.03	5.377	0.001	1206.7	0.3	0.82	0.03	5.0	0.5
523	100	0	0	0	789.8	0.6	0.106	0.002	44	6
523	100	1.03	0.810	0.001	833.4	0.6	0.13	0.01	43.3	0.8
523	100	3.01	2.315	0.001	903.9	0.4	0.146	0.004	37	2
523	100	5.00	3.733	0.003	965.5	0.7	0.172	0.007	32	3
523	100	6.03	4.432	0.001	994.7	0.3	0.185	0.004	32.5	0.8
523	400	0	0	0	822.1	0.3	0.118	0.005	41	3
523	400	1.03	0.8383	0.0004	862.4	0.4	0.14	0.01	39	3
523	400	3.01	2.386	0.001	931.4	0.2	0.152	0.001	32	6
523	400	5.00	3.833	0.001	991.5	0.3	0.184	0.005	31	3
523	400	6.03	4.546	0.001	1020.3	0.3	0.197	0.005	31	2
523	1000	0	0	0	867.9	0.2	0.130	0.002	34	2
523	1000	1.03	0.8813	0.0002	906.7	0.2	0.141	0.005	30	5
523	1000	3.01	2.493	0.001	973.3	0.3	0.169	0.004	30	2
523	1000	5.00	3.990	0.001	1032.2	0.3	0.19	0.01	27.4	0.5
523	1000	6.03	4.725	0.001	1060.4	0.3	0.213	0.005	27	1
723	400	0	0	0	352	2	0.042	0.001	298	9
723	400	1.03	0.431	0.002	443	2	0.051	0.003	225	6
723	400	3.01	1.448	0.006	565	2	0.065	0.002	162	6
723	400	5.00	2.547	0.007	659	2	0.078	0.002	123	7

**Table S11 continued from previous page**

$T$	$P$	$m_{\text{NaCl}}$	$M_{\text{NaCl}}$	$\sigma_m$	$\rho$	$\sigma_\rho$	$\eta$	$\sigma_\eta$	$D_{\text{H}_2}$	$\sigma_{D_{\text{H}_2}}$
723	400	6.03	3.120	0.007	700	2	0.084	0.001	111	9
723	1000	0	0	0	609.2	0.5	0.072	0.002	112	3
723	1000	1.03	0.6409	0.0003	659.3	0.3	0.083	0.006	101	3
723	1000	3.01	1.888	0.003	737	1	0.092	0.003	88	1
723	1000	5.00	3.097	0.002	801.2	0.5	0.105	0.003	79	2
723	1000	6.03	3.706	0.003	831.7	0.6	0.111	0.002	74	2

Table S12: Results of MD simulations used to compute self-diffusivities of  $\text{H}_2$  in aqueous NaCl solutions as computed using the NaCl Madrid-2019<sup>7</sup> force field, the TIP4P/2005<sup>1</sup>  $\text{H}_2\text{O}$  force field, and the Vrabec<sup>3</sup>  $\text{H}_2$  force field. The densities  $\rho$ , viscosities  $\eta$ , and  $\text{H}_2$  finite-size corrected<sup>10</sup> self-diffusion coefficients  $D_{\text{H}_2}$  for a wide range of temperatures  $T$ , pressures  $P$ , NaCl molalities  $m_{\text{NaCl}}$ , and corresponding molarities  $M_{\text{NaCl}}$ .  $T$  is in units of K,  $P$  is in units of bar,  $m_{\text{NaCl}}$  is in units of mol NaCl/kg  $\text{H}_2\text{O}$ ,  $M_{\text{NaCl}}$  is in units of mol NaCl/L solution,  $\rho$  is in units of kg/m<sup>3</sup>,  $\eta$  is in units of mPa·s and  $D$  is in units of 10<sup>-9</sup> m<sup>2</sup>/s.  $\sigma_x$  is the uncertainty of quantity  $x$ . Uncertainties in pressure and temperature are zero as these are imposed in the simulations (*NPT* ensemble).

$T$	$P$	$m_{\text{NaCl}}$	$M_{\text{NaCl}}$	$\sigma_M$	$\rho$	$\sigma_\rho$	$\eta$	$\sigma_\eta$	$D_{\text{H}_2}$	$\sigma_{D_{\text{H}_2}}$
298	1	1.03	1.0050	0.0003	1034.0	0.4	1.02	0.05	3.9	0.5
298	1	3.01	2.825	0.001	1103.0	0.5	1.43	0.09	2.8	0.3
298	1	5.00	4.498	0.002	1163.5	0.5	2.1	0.1	2.2	0.3
298	10	1.03	1.0050	0.0002	1034.3	0.2	1.1	0.1	3.6	0.3
298	10	3.01	2.825	0.001	1103.1	0.4	1.52	0.08	3.0	0.2
298	10	5.00	4.496	0.002	1163.1	0.4	2.0	0.1	2.1	0.2
298	100	1.03	1.0090	0.0002	1038.2	0.2	1.01	0.05	3.8	0.2
298	100	3.01	2.835	0.001	1107.0	0.5	1.43	0.03	2.9	0.3
298	100	5.00	4.509	0.002	1166.3	0.6	2.1	0.1	2.1	0.1
298	400	1.03	1.0210	0.0001	1050.2	0.1	0.9	0.1	3.4	0.3
298	400	3.01	2.862	0.001	1117.5	0.6	1.4	0.1	2.7	0.2
298	400	5.00	4.548	0.002	1176.5	0.6	2.12	0.07	2.1	0.2
298	1000	1.03	1.0430	0.0004	1073.2	0.5	1.02	0.03	2.9	0.4
298	1000	3.01	2.9160	0.0007	1138.3	0.3	1.6	0.2	2.1	0.6
298	1000	5.00	4.622	0.002	1195.6	0.5	2.2	0.1	1.7	0.1
343	1	1.03	0.9823	0.0003	1010.6	0.3	0.47	0.02	8.5	0.4
343	1	3.01	2.7540	0.0008	1075.3	0.3	0.64	0.02	6.9	0.4
343	1	5.00	4.378	0.001	1132.4	0.3	0.84	0.02	5.2	0.1
343	10	1.03	0.9827	0.0001	1011.0	0.1	0.48	0.02	8.5	0.5
343	10	3.01	2.7560	0.0007	1075.8	0.3	0.62	0.03	6.9	0.6
343	10	5.00	4.380	0.001	1133.1	0.4	0.9	0.1	5.3	0.3
343	100	1.03	0.9864	0.0003	1014.8	0.3	0.48	0.02	8.3	0.2
343	100	3.01	2.7650	0.0004	1079.5	0.1	0.65	0.05	5.9	0.8
343	100	5.00	4.394	0.001	1136.7	0.3	0.81	0.02	5.1	0.5

**Table S12 continued from previous page**

$T$	$P$	$m_{\text{NaCl}}$	$M_{\text{NaCl}}$	$\sigma_m$	$\rho$	$\sigma_\rho$	$\eta$	$\sigma_\eta$	$D_{\text{H}_2}$	$\sigma_{D_{\text{H}_2}}$
343	400	1.03	0.9989	0.0001	1027.7	0.1	0.51	0.06	7.5	0.6
343	400	3.01	2.7960	0.0003	1091.6	0.1	0.65	0.04	6.0	0.6
343	400	5.00	4.4370	0.0007	1147.6	0.2	0.9	0.1	5.0	0.5
343	1000	1.03	1.0210	0.0001	1050.6	0.1	0.51	0.01	7	1
343	1000	3.01	2.8500	0.0006	1112.8	0.2	0.67	0.06	6.3	0.8
343	1000	5.00	4.5160	0.0003	1168.1	0.1	0.86	0.04	4.3	0.3
523	100	1.03	0.8119	0.0003	835.3	0.3	0.123	0.003	42	2
523	100	3.01	2.320	0.001	905.6	0.6	0.155	0.003	32	3
523	100	5.00	3.731	0.001	965.2	0.3	0.20	0.01	31.9	0.7
523	400	1.03	0.8393	0.0002	863.5	0.2	0.134	0.001	39	1
523	400	3.01	2.3840	0.0005	930.8	0.2	0.164	0.002	32.9	0.6
523	400	5.00	3.817	0.001	987.5	0.3	0.198	0.005	30	1
523	1000	1.03	0.8808	0.0002	906.2	0.2	0.15	0.01	33.2	0.6
523	1000	3.01	2.4830	0.0006	969.4	0.2	0.183	0.005	29	1
523	1000	5.00	3.9570	0.0005	1023.5	0.1	0.217	0.007	24	2
723	400	1.03	0.451	0.001	464	1	0.0516	0.0002	204	5
723	400	3.01	1.541	0.006	602	2	0.070	0.001	128	9
723	400	5.00	2.692	0.001	696.3	0.3	0.091	0.002	99	6
723	1000	1.03	0.6459	0.0007	664.5	0.7	0.082	0.003	95	3
723	1000	3.01	1.910	0.001	745.6	0.5	0.098	0.001	82	3
723	1000	5.00	3.134	0.002	810.8	0.4	0.1163	0.0007	72.8	0.8

Table S13: Results of the CFCMC simulations using the NaCl Madrid-2019 force field,<sup>7</sup> TIP4P/2005<sup>1</sup> H<sub>2</sub>O force field and Marx<sup>2</sup> H<sub>2</sub> force field. The fluid densities  $\rho$ , infinite dilution chemical potentials  $\mu^{\text{ex}}$  of H<sub>2</sub>, the solubilities of H<sub>2</sub>  $s_{\text{H}_2}$ , and mole fractions  $x_{\text{H}_2}$  are reported for a wide range of temperatures  $T$ , pressures  $P$ , and NaCl molalities  $m_{\text{NaCl}}$ , and corresponding molarities  $M_{\text{NaCl}}$ . The standard deviations  $\sigma$  are reported.  $T$  is in units of K,  $P$  is in units of bar,  $m_{\text{NaCl}}$  is in units of mol NaCl/kg water,  $M_{\text{NaCl}}$  is in units of mol NaCl/L solution,  $\rho$  is in units of kg/m<sup>3</sup>,  $\mu^{\text{ex}}$  is in units of  $k_{\text{B}}T$ ,  $s_{\text{H}_2}$  is in units of mol/L, and  $x_{\text{H}_2}$  is in units of 10<sup>-4</sup>. Uncertainties in pressure and temperature are zero as these are imposed in the simulations (*NPT* ensemble).

$T$	$P$	$m_{\text{NaCl}}$	$M_{\text{NaCl}}$	$\rho$	$\sigma_{\rho}$	$\mu^{\text{ex}}$	$\sigma_{\mu^{\text{ex}}}$	$s_{\text{H}_2}$	$\sigma_{s_{\text{H}_2}}$	$x_{\text{H}_2}$	$\sigma_{x_{\text{H}_2}}$
298	1	0.00	0.00	995	2	4.03	0.03	0.00072	0.00002	0.130	0.003
298	1	0.93	0.91	1032	2	4.22	0.04	0.00059	0.00002	0.107	0.004
298	1	2.96	2.79	1104	2	4.64	0.06	0.00039	0.00002	0.071	0.004
298	1	5.00	4.51	1166	2	5.04	0.03	0.00026	0.00001	0.048	0.001
298	1	5.93	5.24	1191	3	5.16	0.06	0.00023	0.00001	0.043	0.003
298	10	0.00	0.00	997	2	4.10	0.02	0.00667	0.00012	1.205	0.022
298	10	0.93	0.91	1033	2	4.26	0.03	0.00569	0.00019	1.028	0.034
298	10	2.96	2.79	1104	2	4.67	0.04	0.00377	0.00017	0.686	0.031
298	10	5.00	4.51	1166	2	5.05	0.05	0.00258	0.00012	0.472	0.022
298	10	5.93	5.24	1192	2	5.22	0.05	0.00219	0.00011	0.403	0.021
298	100	0.00	0.00	1000	2	4.13	0.02	0.06696	0.00114	12.050	0.207
298	100	0.93	0.91	1037	2	4.34	0.03	0.05401	0.00165	9.723	0.300
298	100	2.96	2.80	1108	2	4.74	0.03	0.03634	0.00099	6.576	0.184
298	100	5.00	4.52	1170	2	5.13	0.07	0.02463	0.00162	4.493	0.300
298	100	5.93	5.26	1195	2	5.25	0.06	0.02187	0.00138	4.010	0.259
298	400	0.00	0.00	1013	2	4.36	0.01	0.25620	0.00290	45.350	0.506
298	400	0.93	0.92	1049	2	4.58	0.02	0.20550	0.00350	36.450	0.626
298	400	2.96	2.82	1119	2	4.98	0.05	0.13810	0.00729	24.720	1.327
298	400	5.00	4.56	1180	2	5.39	0.04	0.09156	0.00359	16.540	0.654
298	400	5.93	5.30	1204	2	5.45	0.06	0.08646	0.00482	15.710	0.882
298	1000	0.00	0.00	1038	2	4.87	0.04	0.55910	0.02658	96.080	4.627
298	1000	0.93	0.94	1071	1	5.05	0.03	0.46960	0.01277	81.200	2.236
298	1000	2.96	2.87	1138	2	5.42	0.02	0.32260	0.00833	56.540	1.472
298	1000	5.00	4.63	1198	2	5.76	0.06	0.23010	0.01463	40.840	2.608

**Table S13 continued from previous page**

$T$	$P$	$m_{\text{NaCl}}$	$M_{\text{NaCl}}$	$\rho$	$\sigma_\rho$	$\mu^{\text{ex}}$	$\sigma_{\mu^{\text{ex}}}$	$s_{\text{H}_2}$	$\sigma_{s_{\text{H}_2}}$	$x_{\text{H}_2}$	$\sigma_{x_{\text{H}_2}}$
298	1000	5.93	5.38	1223	2	5.96	0.08	0.18870	0.01520	33.700	2.721
323	1	0.00	0.00	987	1	4.05	0.02	0.00065	0.00001	0.119	0.002
323	1	0.93	0.90	1022	1	4.23	0.04	0.00054	0.00002	0.099	0.004
323	1	2.96	2.75	1090	1	4.57	0.03	0.00039	0.00001	0.071	0.002
323	1	5.00	4.45	1150	2	4.90	0.01	0.00028	0.00000	0.051	0.001
323	1	5.93	5.17	1175	2	5.04	0.03	0.00024	0.00001	0.045	0.002
323	10	0.00	0.00	986	1	4.03	0.02	0.00662	0.00015	1.209	0.028
323	10	0.93	0.90	1022	2	4.22	0.04	0.00551	0.00024	1.006	0.045
323	10	2.96	2.75	1090	2	4.58	0.01	0.00382	0.00004	0.704	0.007
323	10	5.00	4.45	1150	2	4.92	0.02	0.00271	0.00005	0.503	0.009
323	10	5.93	5.17	1174	2	5.01	0.02	0.00248	0.00006	0.464	0.011
323	100	0.00	0.00	991	1	4.13	0.02	0.06123	0.00114	11.120	0.212
323	100	0.93	0.90	1025	1	4.29	0.01	0.05240	0.00085	9.536	0.151
323	100	2.96	2.76	1093	1	4.62	0.03	0.03753	0.00106	6.882	0.198
323	100	5.00	4.46	1153	2	4.97	0.02	0.02658	0.00060	4.920	0.112
323	100	5.93	5.18	1178	2	5.09	0.02	0.02346	0.00039	4.362	0.076
323	400	0.00	0.00	1004	2	4.36	0.02	0.23330	0.00415	41.680	0.764
323	400	0.93	0.91	1038	1	4.52	0.01	0.19820	0.00170	35.550	0.308
323	400	2.96	2.79	1105	2	4.88	0.02	0.13920	0.00324	25.210	0.599
323	400	5.00	4.50	1164	1	5.17	0.02	0.10360	0.00254	18.970	0.475
323	400	5.93	5.23	1188	1	5.27	0.03	0.09415	0.00305	17.340	0.560
323	1000	0.00	0.00	1028	1	4.80	0.02	0.53410	0.00889	92.730	1.569
323	1000	0.93	0.93	1060	1	4.97	0.02	0.45170	0.00866	78.960	1.508
323	1000	2.96	2.84	1125	2	5.30	0.01	0.32550	0.00327	57.690	0.577
323	1000	5.00	4.58	1183	1	5.60	0.05	0.23930	0.01221	43.000	2.203
323	1000	5.93	5.31	1207	2	5.71	0.03	0.21620	0.00607	39.090	1.101
343	1	0.00	0.00	976	1	3.99	0.02	0.00065	0.00001	0.120	0.002
343	1	0.93	0.89	1009	1	4.14	0.02	0.00056	0.00001	0.103	0.002
343	1	2.96	2.72	1076	1	4.46	0.02	0.00040	0.00001	0.075	0.002
343	1	5.00	4.39	1135	1	4.75	0.01	0.00030	0.00000	0.057	0.001

**Table S13 continued from previous page**

$T$	$P$	$m_{\text{NaCl}}$	$M_{\text{NaCl}}$	$\rho$	$\sigma_\rho$	$\mu^{\text{ex}}$	$\sigma_{\mu^{\text{ex}}}$	$s_{\text{H}_2}$	$\sigma_{s_{\text{H}_2}}$	$x_{\text{H}_2}$	$\sigma_{x_{\text{H}_2}}$
343	1	5.93	5.10	1160	1	4.88	0.02	0.00027	0.00001	0.050	0.001
343	10	0.00	0.00	976	1	3.98	0.02	0.00656	0.00015	1.211	0.028
343	10	0.93	0.89	1010	1	4.15	0.02	0.00553	0.00011	1.022	0.021
343	10	2.96	2.72	1077	1	4.47	0.02	0.00401	0.00009	0.747	0.016
343	10	5.00	4.39	1135	1	4.75	0.02	0.00303	0.00005	0.570	0.009
343	10	5.93	5.10	1160	2	4.90	0.03	0.00262	0.00007	0.495	0.013
343	100	0.00	0.00	980	1	4.06	0.01	0.06213	0.00077	11.410	0.142
343	100	0.93	0.89	1014	1	4.21	0.03	0.05336	0.00138	9.823	0.259
343	100	2.96	2.73	1081	1	4.53	0.02	0.03859	0.00053	7.156	0.098
343	100	5.00	4.40	1139	2	4.81	0.03	0.02918	0.00082	5.469	0.159
343	100	5.93	5.12	1163	1	4.94	0.01	0.02573	0.00037	4.846	0.071
343	400	0.00	0.00	994	1	4.29	0.02	0.23250	0.00599	41.980	1.094
343	400	0.93	0.90	1026	1	4.44	0.03	0.20190	0.00624	36.600	1.149
343	400	2.96	2.76	1092	2	4.74	0.02	0.14930	0.00347	27.360	0.645
343	400	5.00	4.45	1150	1	5.02	0.02	0.11210	0.00272	20.770	0.514
343	400	5.93	5.17	1174	1	5.14	0.03	0.09975	0.00282	18.580	0.533
343	1000	0.00	0.00	1018	1	4.74	0.01	0.52270	0.00715	91.680	1.275
343	1000	0.93	0.92	1050	1	4.88	0.02	0.45230	0.00867	79.830	1.543
343	1000	2.96	2.81	1114	1	5.15	0.03	0.34530	0.00918	61.820	1.651
343	1000	5.00	4.52	1170	1	5.44	0.02	0.26020	0.00561	47.260	1.033
343	1000	5.93	5.25	1194	1	5.57	0.01	0.22730	0.00293	41.530	0.539
363	1	0.00	0.00	962	1	3.88	0.01	0.00068	0.00001	0.128	0.002
363	1	0.93	0.87	996	2	4.04	0.02	0.00058	0.00001	0.109	0.002
363	1	2.96	2.68	1062	1	4.33	0.03	0.00044	0.00001	0.082	0.002
363	1	5.00	4.33	1120	1	4.59	0.02	0.00034	0.00001	0.064	0.001
363	1	5.93	5.03	1144	1	4.70	0.02	0.00030	0.00001	0.058	0.001
363	10	0.00	0.00	963	1	3.88	0.01	0.00681	0.00009	1.275	0.017
363	10	0.93	0.87	996	1	4.04	0.01	0.00585	0.00004	1.096	0.007
363	10	2.96	2.68	1063	1	4.34	0.02	0.00434	0.00007	0.820	0.014
363	10	5.00	4.33	1121	1	4.60	0.04	0.00333	0.00012	0.635	0.024

**Table S13 continued from previous page**

$T$	$P$	$m_{\text{NaCl}}$	$M_{\text{NaCl}}$	$\rho$	$\sigma_\rho$	$\mu^{\text{ex}}$	$\sigma_{\mu^{\text{ex}}}$	$s_{\text{H}_2}$	$\sigma_{s_{\text{H}_2}}$	$x_{\text{H}_2}$	$\sigma_{x_{\text{H}_2}}$
363	10	5.93	5.03	1144	1	4.70	0.03	0.00302	0.00008	0.579	0.016
363	100	0.00	0.00	967	1	3.95	0.01	0.06542	0.00048	12.180	0.092
363	100	0.93	0.88	1000	1	4.09	0.02	0.05661	0.00138	10.560	0.262
363	100	2.96	2.69	1066	1	4.39	0.01	0.04189	0.00053	7.879	0.103
363	100	5.00	4.35	1124	1	4.66	0.02	0.03191	0.00063	6.059	0.122
363	100	5.93	5.05	1148	1	4.78	0.01	0.02840	0.00032	5.417	0.062
363	400	0.00	0.00	981	1	4.18	0.02	0.24340	0.00504	44.500	0.945
363	400	0.93	0.89	1014	1	4.33	0.02	0.20900	0.00410	38.370	0.756
363	400	2.96	2.72	1078	2	4.59	0.04	0.16090	0.00679	29.850	1.292
363	400	5.00	4.39	1135	1	4.88	0.03	0.12140	0.00339	22.770	0.653
363	400	5.93	5.10	1159	1	4.99	0.01	0.10810	0.00129	20.400	0.247
363	1000	0.00	0.00	1006	1	4.61	0.01	0.54840	0.00619	97.300	1.110
363	1000	0.93	0.91	1037	1	4.75	0.02	0.47870	0.01033	85.470	1.862
363	1000	2.96	2.78	1101	1	5.02	0.02	0.36540	0.00707	66.160	1.266
363	1000	5.00	4.47	1157	1	5.28	0.01	0.28160	0.00435	51.720	0.805
363	1000	5.93	5.19	1180	1	5.39	0.03	0.25170	0.00623	46.520	1.172

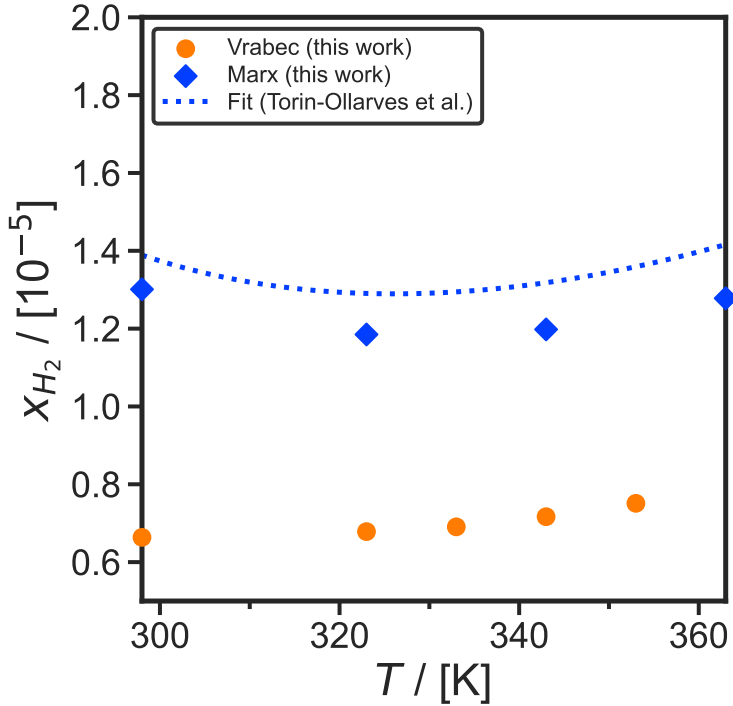


Figure S1: Computed solubilities of  $H_2$  in pure water using the TIP4P/2005<sup>1</sup>  $H_2O$  force field in combination with either the Marx<sup>2</sup>  $H_2$  force field (diamonds) or the Vrabec<sup>3</sup> force field (circles) as a function of temperature  $T$  at a  $H_2$  partial pressure of 1 bar. The dashed lines represent the experimental correlation provided by Torín-Ollarves and Trusler<sup>4</sup>.

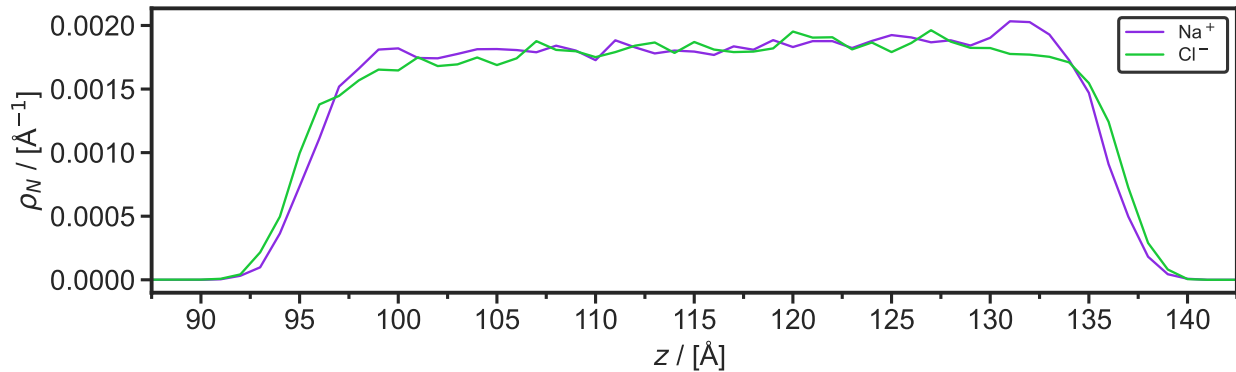


Figure S2: Number density profile  $\rho_N$  in the  $z$ -direction of  $Na^+$  and  $Cl^-$  from a Molecular Dynamics simulation to calculate the interfacial tension of  $H_2$  and a aqueous  $NaCl$  solution (3 mol/kg  $H_2O$ ) at 343 K and 100 bar. Only the aqueous  $NaCl$  solution and the interfaces with  $H_2$  are shown, which is part of the full simulation box. The full box is shown in Figure 1 of the main text of the manuscript. The profile is averaged for 5 ns.  $z$  is the direction perpendicular to the interface.

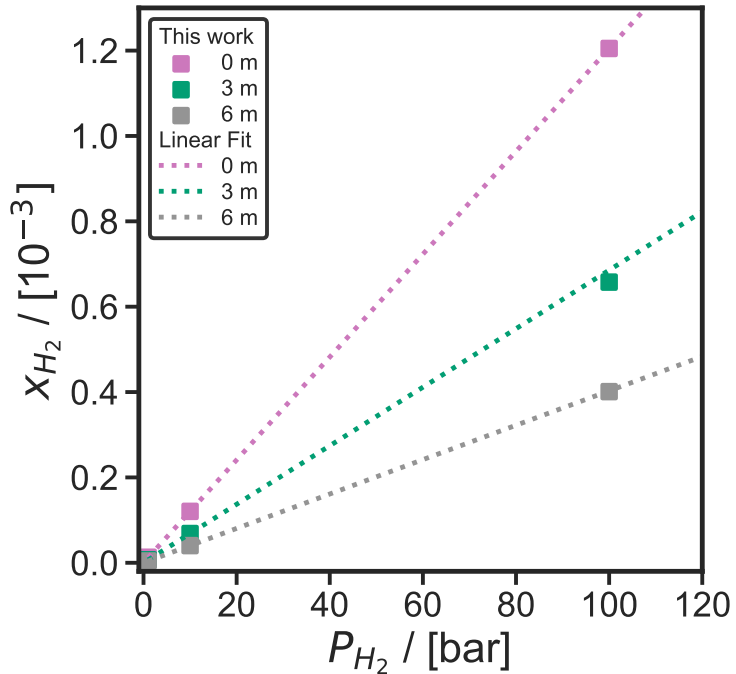


Figure S3: Computed solubilities of  $H_2$  in aqueous NaCl solutions as a function of  $H_2$  partial pressure at different molalities ( $m$ ) of 0, 3, and 6 mol NaCl / kg  $H_2O$ . The NaCl Madrid-2019<sup>7</sup> force field is used in combination with the TIP4P/2005  $H_2O$  force field<sup>1</sup> and the  $H_2$  Marx force field.<sup>2</sup> Eq. 6-9 of the main text are used to compute the solubilities of  $H_2$  in the aqueous solution. The solubilities are fitted by a linear function (shown as dotted lines) as described by Eq. 8 (Henry regime). Clearly, Eq. 8 is valid for  $H_2$  partial pressures ranging from 1-100 bar.

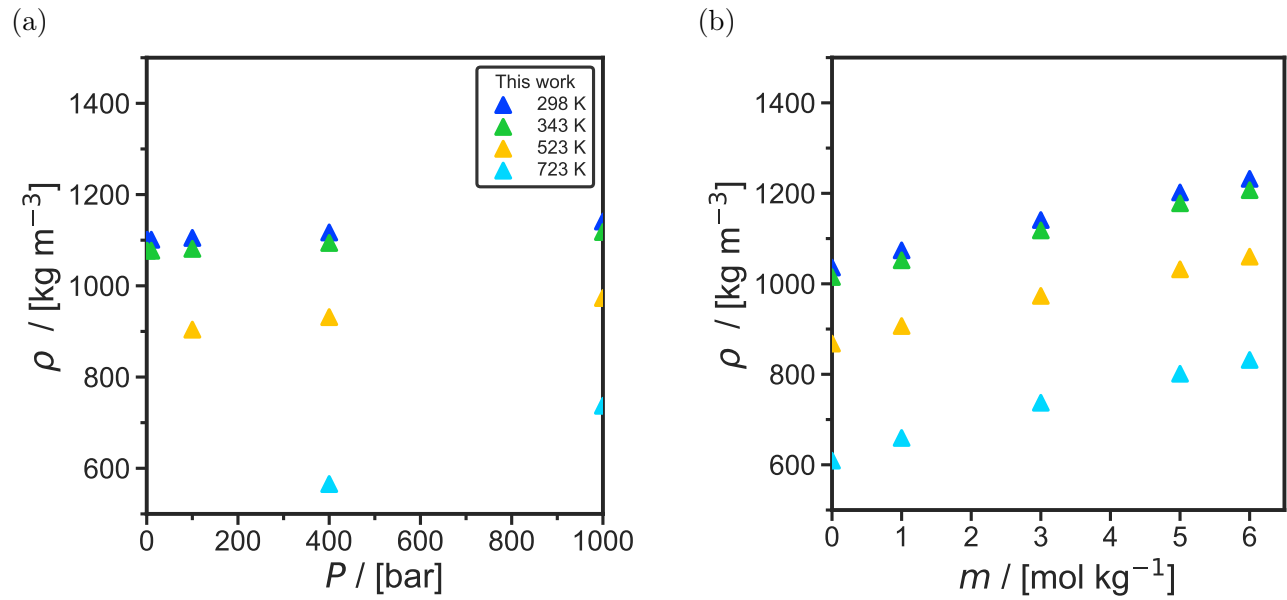


Figure S4: Densities of aqueous sodium chloride solutions as a function of (a) pressure for a solution molality of 3 mol/kg water and (b) sodium chloride molality at a pressure of 1000 bar computed using the NaCl Madrid-Transport<sup>5,6</sup> force field, the TIP4P/2005<sup>1</sup> water force field, and the Vrabec<sup>3</sup> hydrogen force field.

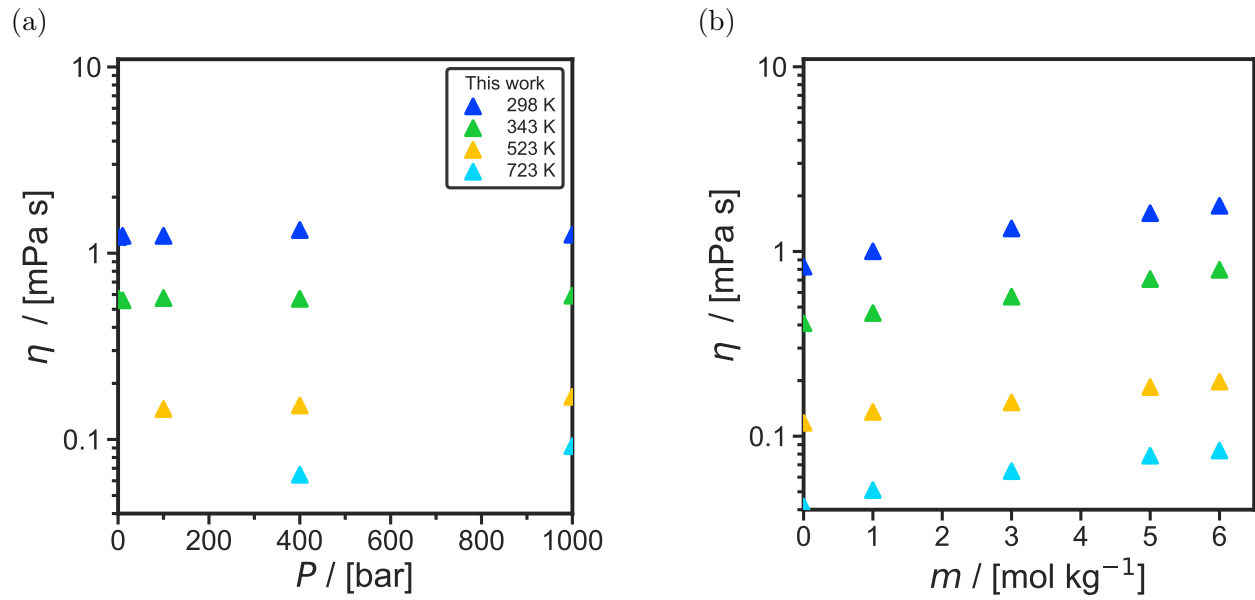


Figure S5: Viscosities of aqueous sodium chloride solutions as a function of (a) pressure at a solution molality of 3 mol NaCl/kg water and (b) sodium chloride molality computed at a pressure of 400 bar using the NaCl Madrid-Transport<sup>5,6</sup> force field, the TIP4P/2005<sup>1</sup> water force field, and the Vrabec<sup>3</sup> hydrogen force field.

## Literature Cited

- (1) Abascal, J. L.; Vega, C. A general purpose model for the condensed phases of water: TIP4P/2005. *J. Chem. Phys.* **2005**, *123*, 234505.
- (2) Marx, D.; Nielaba, P. Path-integral Monte Carlo techniques for rotational motion in two dimensions: Quenched, annealed, and no-spin quantum-statistical averages. *Phys. Rev. A* **1992**, *45*, 8968.
- (3) Köster, A.; Thol, M.; Vrabec, J. Molecular Models for the Hydrogen Age: Hydrogen, Nitrogen, Oxygen, Argon, and Water. *J. Chem. Eng. Data* **2018**, *63*, 305–320.
- (4) Torín-Ollarves, G. A.; Trusler, J. M. Solubility of hydrogen in sodium chloride brine at high pressures. *Fluid Phase Equilib.* **2021**, *539*, 113025.
- (5) Blazquez, S.; Conde, M. M.; Vega, C. Submitted. **2023**, Uploaded as Supporting Information for review only.
- (6) Habibi, P.; Rahbari, A.; Blazquez, S.; Vega, C.; Dey, P.; Vlugt, T. J. H.; Moulton, O. A. A New Force Field for OH<sup>-</sup> for Computing Thermodynamic and Transport Properties of H<sub>2</sub> and O<sub>2</sub> in Aqueous NaOH and KOH Solutions. *J. Phys. Chem. B* **2022**, *126*, 9376–9387.
- (7) Zeron, I. M.; Abascal, J. L. F.; Vega, C. A force field of Li<sup>+</sup>, Na<sup>+</sup>, K<sup>+</sup>, Mg<sup>2+</sup>, Ca<sup>+</sup>, Cl<sup>-</sup>, and SO<sub>4</sub><sup>2-</sup> in aqueous solution based on the TIP4P/2005 water model and scaled charges for the ions. *J. Chem. Phys.* **2019**, *151*, 104501.
- (8) Laliberté, M.; Cooper, W. E. Model for calculating the density of aqueous electrolyte solutions. *J. Chem. Eng. Data* **2004**, *49*, 1141–1151.

- (9) Laliberté, M. Model for calculating the viscosity of aqueous solutions. *J. Chem. Eng. Data* **2007**, *52*, 321–335.
- (10) Celebi, A. T.; Jamali, S. H.; Bardow, A.; Vlugt, T. J. H.; Mourtos, O. A. Finite-size effects of diffusion coefficients computed from molecular dynamics: a review of what we have learned so far. *Mol. Simul.* **2021**, *47*, 831–845.